Geoderma 467 (2026) 117749

Contents lists available at ScienceDirect

Geoderma

journal homepage: www.elsevier.com/locate/geoderma

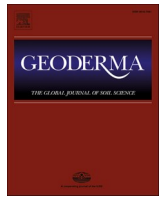

Combined diffuse reflectance spectroscopy and digital soil mapping for soil assessment in smallholder farms

Naveen K. Purushothaman [a], Kaushal K. Garg [b], Nagaraju Budama [b], Venkataradha Akuraju [b], K.H. Anantha [b], Ramesh Singh [b,c], M.L. Jat [b,c], Bhabani S. Das [a,*]

[a] Agricultural and Food Engineering Department, Indian Institute of Technology Kharagpur, 721302 West Bengal, India
[b] International Crops Research Institute for the Semi-Arid Tropics, Patancheru 502324, Telangana, India
[c] Indian Council of Agricultural Research, New Delhi, India

ARTICLE INFO

Handling editor: Jingyi Huang

Keywords:
Chemometric modelling
Cubist
Environmental covariates
Feature selection
Quantile regression forest

ABSTRACT

Diffuse reflectance spectroscopy (DRS) and digital soil mapping (DSM) offer opportunities to rapidly assess soil in large areas. Specifically, the combined DRS-DSM modelling pipeline may be used to create soil test recommendations for every smallholder farm in a given region although comprehensive testing of such a pipeline is rarely attempted. With multi-year and multi-site soil spectral data from the smallholder farms of the Bundelkhand region, we evaluated the DRS-DSM pipeline for estimating soil properties and making nutrient recommendation for every smallholder farm both within and outside the DRS calibration zones. Specifically, we compared both measured and DRS-estimated soil properties as inputs in DSM approaches using 1112, 607, and 407 soil samples collected during 2018 (T_{2018}: calibration zone), 2021 (T_{2021}: within the calibration zone), and 2022 (T_{2022}: outside the calibration zone), respectively, for estimating 17 soil parameters and their soil test crop response (STCR) ratings. For T_{2022} samples, DRS models calibrated within the calibration zone accurately predicted 7 out of 17 soil properties with Lin's concordance correlation coefficients (LCCC) exceeding 0.6. Spiking these datasets with T_{2022} data further improved predictions to 10 properties and reduced errors by 3–29%. In T_{2021} dataset, both measured property- and DRS-based DSM approaches achieved comparable accuracy. Estimated STCR rating accuracies for the DRS-DSM pipeline exceeded 70% for 9 out of 13 properties suggesting that these two emerging technologies may be combined to make nutrient recommendations across smallholder farms within a given region.

1. Introduction

Soil testing is crucial for increasing agricultural production and farm income. With the conventional wet chemistry-based soil testing generally time-consuming and tedious (Stenberg et al., 2010), the diffuse reflectance spectroscopy (DRS) has emerged as a rapid (Dalal and Henry, 1986) and reliable soil testing approach (Viscarra Rossel et al., 2006; Grinand et al., 2012; Viscarra Rossel et al., 2022). Specifically, recent studies show that the DRS approach may be used to test as many as 60% of new soil samples with > 70% accuracy in smallholder farms spreading across large regions (Purushothaman et al., 2024) and even in managed cocoa production systems (Purushothaman et al., 2025). A specific limitation of the DRS approach is that the spectral reflectance (*R*) data for a soil sample must be collected (Ge et al., 2007) for estimating a target soil property at any unsampled location. Such a limitation may be tackled with the digital soil mapping (DSM) approach, in which soil properties at an unsampled location are estimated by combining measured soil properties, different covariates and a suitable predictive model (McBratney et al., 2003). Rapid developments in efficient machine learning (Wadoux et al., 2020) and deep learning (Behrens et al., 2018; Padarian et al., 2019) approaches offer promise for reliably estimating soil properties at unsampled locations through the DSM approach.

A specific limitation with the DSM approach is the prohibitive cost of collecting and analysing a large number of soil samples, which is needed for capturing soil's inherent spatial variability. For many developing countries, the number of smallholder farms is increasing with the decrease in their individual farm sizes (Hansen, 2024). As farmers

* Corresponding author.
E-mail addresses: kaushal.garg@icrisat.org (K.K. Garg), Nagaraju.Budama@icrisat.org (N. Budama), Venkataradha.Akuraju@icrisat.org (V. Akuraju), Anantha.kanugod@icrisat.org (K.H. Anantha), Ramesh.Singh@icrisat.org (R. Singh), DG.ICAR@nic.in (M.L. Jat), bsdas@agfe.iitkgp.ac.in (B.S. Das).

https://doi.org/10.1016/j.geoderma.2026.117749
Received 14 September 2025; Received in revised form 19 February 2026; Accepted 20 February 2026

micro-manage these farms, local-scale management may change soil properties even at shorter time scales (Das et al., 2015) requiring frequent soil testing for the precision management of different agricultural inputs. From an administrative standpoint, frequent soil testing is also required for quantifying the amount of organic or inorganic fertilizers needed for a specific region, which influences both the supply chain of nutrient sources and associated decision making. Both the DRS and DSM approaches may, in turn, be combined (Viscarra Rossel and McBratney, 2008; Somarathna et al., 2018; Wadoux et al., 2019; Chen et al., 2023) to leverage their individual strengths although a key question remains as to what extent these two technologies may be combined to meet the frequent soil testing needs of smallholder farms and of local administrative units.

Studies combining DRS and DSM approaches are few, with most studies focused on the assessment of soil organic carbon (SOC) contents (Table S1). Some of the initial studies used geostatistical approaches (e.g., OK: ordinary kriging, RK: regression kriging, and co-kriging) to map residuals obtained using the DRS-estimated soil properties at small agricultural farm (Ge et al., 2007; Brodský et al., 2013) and watershed (Lamsal, 2009) scales. Subsequently, machine learning models were frequently used in DRS and the resulting DRS-estimated soil properties were combined with DSM to estimate both soil properties and their estimation uncertainties (Viscarra Rossel et al., 2014; Ma et al., 2021; Dai et al., 2025). More recently, Chen et al. (2023) used the DRS dataset ($n = 2036$) from the French Soil Monitoring Network (RMQS; Jolivet et al., 2006) and soil property dataset ($n = 2685$) from the Land Use and Coverage Area frame Survey (LUCAS) for France (Tóth et al., 2013). Their study demonstrated that the uncertainty in the DSM-based estimation of SOC, clay and soil pH can be reduced. This reduction in the uncertainty can be achieved when a sufficiently large proportion of DRS-inferred soil data is used and the DRS models have high estimation accuracy. Collectively, these studies demonstrated that machine-learning approaches outperform purely statistical or geostatistical models and enable soil mapping across broad spatial scales, although similar studies using multi-temporal soil data across different calibration zones are rarely reported. Specifically, no previous study has addressed both spatial and temporal transferability of DRS-DSM pipeline for estimating multiple soil properties in smallholder farms.

Applicability of DRS models for analysing new samples (spatio-temporal transferability) is influenced by several factors including calibration sample size, environmental conditions, parent material, confounding soil properties, measurement quality, pre-processing protocols, and the modelling approach adopted among others (Guerrero et al., 2010; Minasny et al., 2009; Brunet et al., 2007; Liu et al., 2018; Grunwald et al., 2018). Sample similarity and the relationships between chromophores and non-chromophores in a soil sample further determine the predictive performance of DRS applicability (Long et al., 2023; Sarathjith et al., 2014). Although several DRS studies have evaluated model performance, most focus on validation within the calibration zone and rarely test on the outside calibration zone. Similarly, previous DRS-based DSM studies generally used calibrated DRS models as inputs for DSM without examining their applicability to outside calibration zone samples. Consequently, the transferability of DRS predictions to independent locations and their impact on DSM outputs remain largely unexplored.

This study is built upon the doubling farmers' income project implemented in the Bundelkhand region of Uttar Pradesh, where we developed soil spectral libraries (SSL) and showed that calibrated DRS models may be successfully used for testing soil samples collected during the same year from the same calibration zones (Majeed et al., 2023) and in samples collected at a future time but from the same calibration zones (Purushothaman et al., 2024; 2025). These studies provided evidence supporting the use of the DRS approach for soil testing in smallholder farm-scale for making soil management decisions. However, the efficacy of these calibrated models for predicting future samples collected outside the calibration zones remain untested. Second, the availability of multi-year and georeferenced soil data from the smallholder farms of the Bundelkhand region provides an opportunity to integrate both DRS and DSM approaches such that soil test-based recommendations are available for every farm within the Bundelkhand region. We hypothesize that calibrated DRS models may reliably be used to estimate soil properties in future samples collected outside a specific calibration zone within a given region, and that the DRS-estimated soil properties be integrated with a suitable DSM approach to map soil properties for every smallholder farm both inside and outside calibration zones of the DRS models. Furthermore, we hypothesize that the combined DRS-DSM pipeline may be used for developing site-specific soil test crop response (STCR) ratings to support actionable nutrient recommendations at the scale of smallholder farms. Thus, the major objectives of this study are to a) test the efficacy of calibrated DRS models for soil testing in future samples collected outside the calibration zones, b) test if the DRS-estimated soil properties may be digitally-mapped for estimating soil properties both within and outside the calibration zones, and c) evaluate a DRS-supported DSM framework (DRS-DSM pipeline) for developing STCR ratings needed for making nutrient recommendations at farmers' field scales. Specifically, we test the scale-up strategy where the DRS-estimated soil properties and their STCR ratings are digitally mapped and compared with DSM products derived from conventionally measured (wet chemistry) soil parameters.

2. Materials and methods

2.1. Study area and soil sampling

The International Crop Research Institute for the Semi-Arid Tropics (ICRISAT), Patancheru, Hyderabad, implemented a mesoscale land rehabilitation project (Garg et al., 2020) across 7 districts (Jhansi, Jalaun, Lalitpur, Mahoba, Hamirpur, Banda, and Chitrakoot) of the Bundelkhand region (Fig. 1). As a part of land rehabilitation strategy, intensive soil sampling was carried out in selected smallholder farms across these districts for making STCR-based nutrient recommendation. Accordingly, 1112 surface (0–15 cm depth) soil samples were collected during May-June 2018 (T_{2018} dataset) by selecting 2–3 villages from 8 different administrative development blocks (also called as tehsil) from these 7 districts (Majeed et al., 2023). This baseline soil sampling covered 20 villages. Subsequently, 607 soil samples were collected from randomly selected farms from these 20 villages during March-April 2021 (T_{2021} dataset) such that their sampling locations differed from those of T_{2018}. Thus, both T_{2018} and T_{2021} sampling locations are interspersed within the same region of sampling although no samples of these two sampling campaigns shared any common sampling location. The third dataset used in this study consisted of surface soil samples collected during March-April 2022 (T_{2022} dataset) from 407 farmers' fields distributed over 40 contiguous villages (area: 280 km^2) of the Tahrauli tehsil of the Jhansi district (Fig. S1). The Tahrauli tehsil is located away from each of the 8 tehsils considered for generating T_{2018} and T_{2021} database (Fig. 1). While T_{2018} samples served as a regional-scale calibration dataset prior to the initiation of land rehabilitation activities, the T_{2021} samples served as a temporally-independent dataset collected from within the same T_{2018} sampling zone (i.e., within the primary calibration zone). In contrast, the T_{2022} samples fell outside the T_{2018} and T_{2021} dataset and were collected at a different time. Moreover, the Tahrauli site was selected because of its strategic position. Geologically, the northern part the Bundelkhand region covering Jalaun, Hamirpur, Banda and Chitrakoot districts is of quaternary sedimentary geological (QSG) origin (Wandrey and Law, 1997; Sharma and Mondal, 2018) while the southern districts of Jhansi and Lalitpur have Precambrian crust geology (PCG). Although located within the PCG setting, Tahrauli lies very close to the boundary of QSG origin with the possibility of having samples of both PCG and QSG origin. Thus, the T_{2018} dataset serves as a regional-scale and baseline dataset covering both PCG and QSG formations. The T_{2021} dataset serves as a temporally-independent

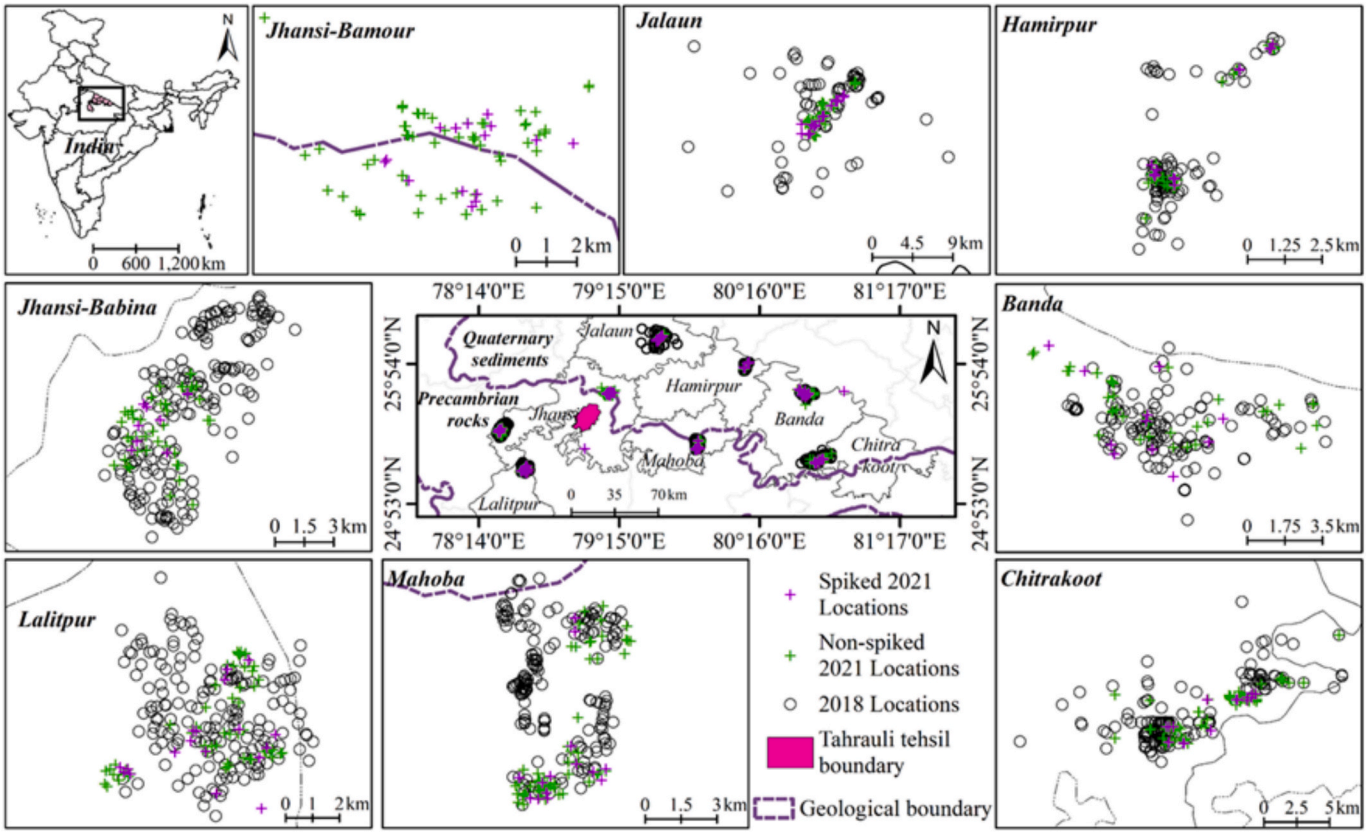

Fig. 1. Locations of soil samples collected from selected development blocks of the Bundelkhand region during 2018 and 2021 (spiked and non-spiked samples) along with the Tahrauli tehsil boundary; sampling locations for Tahrauli tehsil collected during 2022 are shown in the Fig. S1.

dataset with its sampling locations distributed within the sampling zones of the T_{2018} dataset. The T_{2022} dataset may be considered as spatially- and temporally-independent dataset with its sampled locations distributed completely outside the sampling zones of T_{2018} and T_{2021} datasets (i.e., outside the primary calibration zone). In summary, the T_{2018} dataset serves as a regional SSL for the Bundelkhand region while the T_{2021} dataset is a temporally-independent regional SSL developed from within the same calibration zone of T_{2018}. In contrast, the T_{2022} dataset serves as both spatially- and temporally-independent test data source for evaluating the spatio-temporal transferability of the DRS approach. Together, these three dataset may be used for evaluating the overall utility of a combined DRS-DSM pipeline for meeting the soil testing needs of every smallholder farm within a targeted administrative unit (e.g., tehsil or village) when a regional SSL is available.

Dominantly Indo-Gangetic alluviums on the north and granite-gneisses on the south, Bundelkhand region shows four distinct soil orders: Entisols, Alfisols, Inceptisols, and Vertisols (Kumar et al., 2021). The climate is sub-humid and characterized by a hot dry summer and cold winter. Average annual rainfall in the Jhansi district is in the order of 850 mm with about 91% caused by the southwest monsoon during the rainy season (Singh et al., 2013). January is the coldest month of the year with the mean daily maximum and minimum temperature of 24.1 °C and 9.2 °C, respectively. May is the hottest month with mean daily maximum temperature of 42.6 °C and minimum of 28.8 °C (Singh et al., 2013). With about 550–800 mm average annual rainfall (Singh et al., 2022) and hot summers with maximum temperature often exceeding 45–47 °C (Kumar et al., 2021), farmers in this semi-arid climate rely primarily on rainfed agriculture.

2.2. Measurement of soil parameters and spectral reflectance

Collected samples were air-dried and < 2 mm soil fractions were separated for analyzing different soil properties. Altogether, 17 soil parameters such as coarse sand, fine sand, clay, pH, SOC, electrical conductivity (EC), exchangeable Na, and 10 different plant nutrients (P, K, Ca, Mg, S, Fe, Mn, Cu, Zn, B) were analyzed using standard laboratory methods. Soil mechanical analysis using a Bouyoucos hydrometer was used for estimating soil textural fractions (Sarkar and Haldar, 2005). Soil pH and EC were measured in a 1:2.5 soil:water slurry using pH and EC meters, respectively. The chromic acid digestion method was followed to measure SOC contents (Walkley and Black, 1934). The Olsen's and Bray's methods were used for measuring available P using a continuous auto-analyser (Olsen and Sommers, 1982). Exchangeable cations such as Ca, Mg, Na, and K were extracted using 1 N ammonium acetate (Hanway and Heidel, 1952) and the analytes were measured using a flame photometer (Systronics India Ltd., Ahmedabad, India). Similarly, the diethylenetriamine penta-acetic acid (DTPA) extraction method was followed to extract four micronutrients (Fe, Mn, Cu, and Zn) and the extracts were analysed using an inductively-coupled plasma spectrometer (Model: HD prodigy; Teledyne Leeman Labs, USA). Available B was extracted using hot-water and the colorimetric method was followed for determining its concentration (Keren, 1996).

A portable spectroradiometer (Model: Field spec®4 Hi-Res NG; Malvern Panalytical Ltd., USA) in combination with a turntable was used to collect reflectance spectra of the 2 mm-sieved soil samples over visible to near- and shortwave infrared (VNIR) region (wavelength, λ: 350 to 2500 nm). The turntable is fitted with a halogen bulb as its light source and has a rotating platform (22 rpm) to hold samples at a sampling spot size of 53.2 mm (field of view: ~88 cm^2). We used a borosil glass Petri dish (diameter: 11 cm) to pack about 100 g of processed soil sample. Each Petri dish was completely filled with soil sample; the

surface was levelled using a thin glass plate to avoid soil compression. Fig. S2 shows the picture of the packed soil sample and laboratory set up used for collecting soil spectra. For the collection of spectral reflectance data, the spectroradiometer and the halogen bulb were warmed up for one hour before making any measurement. The instrument was optimized for its light source using a Spectralon® white reference panel (Lab sphere, USA) at the beginning of the measurement and after reflectance data were collected for every 30 samples. Thirty scans were averaged to obtain a VNIR spectra for each soil sample.

2.3. Chemometric modelling and digital soil mapping

Before chemometric modelling, each VNIR spectra was clipped to retain reflectance data over 400 nm to 2450 nm (high signal-to-noise ratio) and reflectance values were transformed to absorbance values. Resulting absorption spectra were then smoothed using a second-order Savitzky-Golay smoothing approach (Savitzky and Golay, 1964) with 11 nm window length (Ng et al., 2019; Viscarra Rossel et al., 2024) and resampled at 10 nm interval to reduce collinearity (Viscarra Rossel and Webster, 2012; Luce et al., 2022). Additionally, absorption values were transformed to their standard normal variates (SNV) to minimize scattering effects (Barnes et al., 1989). The *prospectr* package (version 0.2.6; Stevens and Ramirez-Lopez, 2022) from the RStudio (ver. 4.3.1; R Core Team, 2023) was used to implement all these spectral pre-processing steps.

With our primary goal of testing a DRS-DSM pipeline (Fig. 2) for soil testing in every smallholder farm in a given region, we considered T_{2018} dataset as a regional-scale SSL for calibrating chemometric models. Spiking is known to improve the estimating accuracy of DRS models (Shepherd and Walsh 2002; Ng et al., 2022; Zayani et al., 2023). Earlier, Luce et al. (2022) recommended that 20% of test data is adequate for spiking a calibration dataset. Using the T_{2018} and T_{2021} datasets and cLHS algorithm, Purushothaman et al. (2024) conducted a sensitivity analysis by increasing the spiking ratio from 5% to 50% and observed that the root-mean-squared error (RMSE) did not change much when the extent of spiking data was increased beyond 20%. Similar results were also observed for three different cocoa orchards of Papua New Guinea (Purushothaman et al., 2025). Hence, we selected 20% of new samples through cLHS-based subsampling as an operational threshold for selecting spiking dataset for the Bundelkhand region. Accordingly, 20% of the T_{2021} samples were selected through the cLHS approach for spiking the T_{2018} dataset to form an augmented (spiked) regional-scale SSL (hereinafter referred to as $RSLS_{in}$) for calibrating DRS models. The T_{2021} dataset originated from the same neighbourhood of the T_{2018} sampling locations and were collected at a different time period. Hence, the $RSLS_{in}$ dataset contained both the spatial (i.e., primary calibration

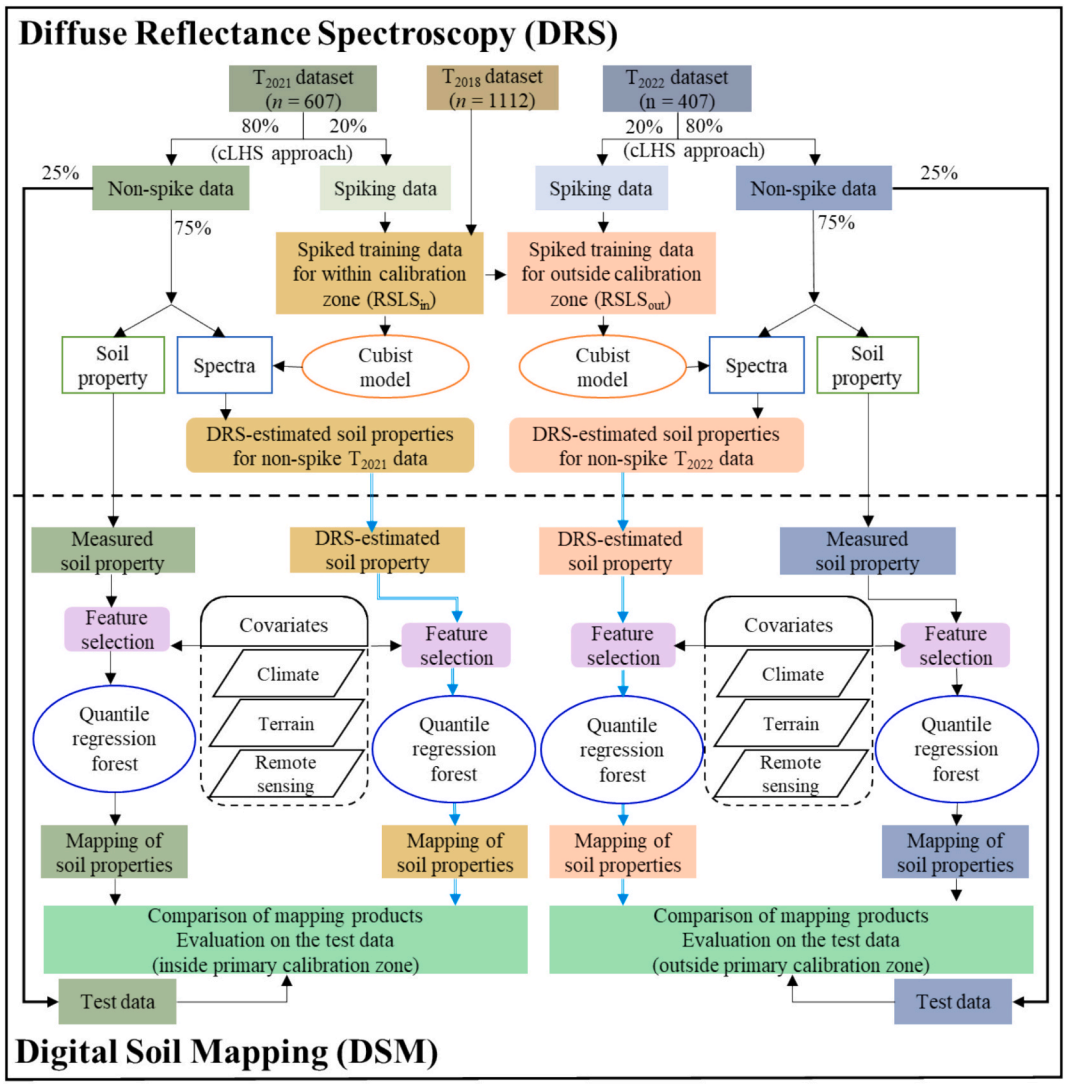

Fig. 2. Flowchart for combined diffuse reflectance spectroscopy (DRS) and digital soil mapping (DSM) framework for estimating soil properties using soil samples collected during 2018 (T_{2018}), 2021 (T_{2021}), and 2022 (T_{2022}).

data from T_{2018}) and spatio-temporal (spiking data from T_{2021}) variations in spectral characteristics of the Bundelkhand region. We calibrated the DRS models using the $RSLS_{in}$ dataset to estimate soil properties in the non-spike samples (i.e., remaining 80%) of the T_{2021}, which originated from the same calibration zone. To examine how a calibrated DRS model from a given calibration zone performs in soil samples collected from outside the calibration zone, we tested the DRS model from $RSLS_{in}$ dataset in the non-spike samples (i.e., 80% of T_{2022} dataset) collected from the Tahrauli tehsil. We also selected 20% of the T_{2022} data through the cLHS approach and merged it with the $RSLS_{in}$ dataset for developing a regional-scale spiked calibration dataset for Tahrauli (hereinafter referred to as $RSLS_{out}$). The $RSLS_{out}$ dataset contained some of the spectral characteristics of soil samples from the Tahrauli tehsil and was used for estimating soil properties in the remaining 80% of soil samples from the T_{2022} dataset (i.e., non-spike T_{2022}). In other words, the DRS models calibrated with the $RSLS_{out}$ dataset were tested on the non-spike T_{2022} dataset, which was originated from outside the primary calibration zones of T_{2018}. Using these two regional-scale SSLs, we estimated 17 different soil properties in the DRS approach by calibrating the Cubist model, which is commonly used in soil spectroscopy (Viscarra Rossel et al., 2016). Calibrated Cubist models were used for estimating soil properties both in the remainder of the T_{2021} and T_{2022} datasets (hereinafter, referred to as non-spike data) for subsequent DSM modelling.

Both measured and DRS-estimated soil properties were used in the SCORPAN approach for developing DSM products for different soil properties using only the non-spike data of the T_{2021} and T_{2022} datasets (i.e., no spiking data were used in DSM modelling). To maintain uniform test datasets, the non-spike data of the T_{2021} and T_{2022} datasets were randomly divided into 75:25 ratio for obtaining training and testing datasets for DSM modelling. Thus, 4 DSM training scenarios were compared by considering measured and DRS-estimated soil properties as calibration dataset for the T_{2021} and T_{2022} non-spike datasets. For each of these cases, measured soil properties in 25% of the non-spike samples were considered as test datasets. Each of the 17 soil parameters was estimated using the quantile regression forest (QRF) model (Meinshausen, 2006), which is a state-of-the-art machine learning algorithm increasingly used in DSM studies (Vaysse and Lagacherie, 2017; Poggio et al., 2021). To implement this approach, we extracted a total of 171 environmental covariates (Table S2) based on the soil-landscape *scorpan* model (McBratney et al., 2003) for generating digital soil maps. Extraction of topographic (terrain) covariates were done using the ~ 90-m multi-error-removed improved-terrain (MERIT) digital elevation model (DEM) data downloaded from the google earth engine (Yamazaki et al., 2017). The MERIT DEM was developed by removing different error components (absolute bias, stripe noise, speckle noise, and tree height bias) from SRTM3 (v2.1) data available from NASA's Shuttle Radar Topography Mission (SRTM) and AW3D-30 m (v1) data available from the Advanced Land Observing Satellite (ALOS) mission from the Japan Aerospace Exploration Agency (JAXA). The terrain-based covariates were extracted from MERIT DEM data using the System for Automated Geoscientific Analyses (SAGA v.9.0.2) software. Different climate-related covariates (mean monthly precipitation, solar radiation, average temperature, maximum temperature, minimum temperature, vapour pressure and wind speed) averaged over 1970 to 2000 (Fick and Hijmans, 2017) were downloaded from the World Climatic Centre (WCLIM V2.1). Additionally, 19 different bioclimatic variables were also used along with the above climate proxies. Similarly, MODIS data (retrieved from MOD13Q1 v6.1) were used to derive mean monthly values for the vegetation-linked parameters of the normalized difference vegetation index (NDVI) and enhanced vegetation index (EVI). With the aim of deriving DSM data products at the smallholder farm scales (~ < 1 ha area), we resampled all covariate data to 10 m spatial resolution.

A parsimonious set of key covariates were determined using the 'Boruta' feature selection algorithm (Kursa and Rudnicki, 2010) to avoid computational complexity and correlation among different covariates while building the QRF model. In this approach, important feature variables are selected by creating different "shadow" attributes (Kursa and Rudnicki, 2010) and the random forest (RF) classification algorithm (Liaw and Wiener, 2002). We used 1000 iterations and maximum Z score criterion in the 'Boruta' package (R software) till the *p*-value reduced to 0.05 during feature selection. Only the top 20 significant covariates were used for each soil parameter for the final DSM modelling to reduce over-fitting (Reddy and Das, 2023). The QRF model was implemented by using 500 trees in the *quantregForest* package in R software (Meinshausen, 2006; Vaysse and Lagacherie, 2017). A grid-search approach in the sequence of 1 to 20 (maximum covariates used in our case) was used to determine the number of variables required to grow each tree (*mtry*).

2.4. Evaluation of model performance

The performance of different predictive models used in developing DRS and DSM products was assessed using the RMSE, bias, and Lin's concordance correlation coefficients (LCCC; Lawrence and Lin, 1989):

$$RMSE = \sqrt{\frac{\sum_{i=1}^{N}(Y_i - \widehat{Y}_i)^2}{N}} \quad (1)$$

$$LCCC = \frac{2\rho\sigma_x\sigma_y}{\sigma_x^2 + \sigma_y^2 + \left(\mu_x - \mu_y\right)^2} \quad (2)$$

where Y_i and $\widehat{Y}_i$ are, respectively, the measured and predicted soil parameter at the i^{th} test location, N is the number of locations, ρ is the Pearson correlation coefficient between Y_i and $\widehat{Y}_i$ values, and μ_x and σ_x^2 and μ_y and σ_y^2 are the means and variances of Y_i and $\widehat{Y}_i$ values, respectively. The bias values were estimated as the difference between the mean value of predicted and measured soil properties. In addition, we also followed Purushothaman et al. (2024) to estimate how soil properties at an unsampled location may be accurately estimated at given threshold levels (T) using the percentage relative error deviation (PRED) from the respective DSM products:

$$\mathrm{PRED(T)} = \left[\frac{1}{n}\sum_{i=1}^{n}\begin{cases} 1 if \dfrac{|Y_i - \widehat{Y}_i|}{Y_i} \le T \\ 0 if \dfrac{|Y_i - \widehat{Y}_i|}{Y_i} > T \end{cases}\right] \times 100 \quad (3)$$

where n is the number of samples at unsampled locations (Shepperd and MacDonell, 2012). In general, large PRED values indicate better estimation accuracy for a given model while T values typically range from 25 to 75% (Silhavy et al., 2021). Earlier, we evaluated PRED(T) values at multiple thresholds (T = 10, 20, 30, 40, and 50) for the same T_{2018} dataset and found that a 30% error threshold provided a consistent and meaningful level of interpretability, with median PRED(30) values exceeding 60% for most soil properties (Purushothaman et al., 2024). Therefore, we calculated PRED values at T = 30 for each of the 17 soil parameters in the current study for consistency and comparability. We also estimated STCR ratings using the three-tier STCR classification scheme (Table S3) generally used for Indian soils (Sendhil et al., 2018). Because the STCR ratings (threshold values) for soil textural fractions and exchangeable Na are not available, we estimated the STCR ratings for the remaining 13 soil parameters using their laboratory-measured values in each soil sample. The STCR rating accuracy (SRA) for each soil parameter in a dataset was then estimated by calculating the percentage of locations for which estimated and laboratory-measured values of the parameter yielded identical STCR ratings:

$$SRA = \frac{Numberofcorrectlyclassifiedsamples}{Totalnumberofsamples} \times 100 \quad (4)$$

For the uncertainty quantification in the DSM approach, both the lower (5%) and upper (95%) limits of the 90% prediction interval (Vaysse and Lagacherie, 2017; Reddy and Das, 2023) were mapped for each variable. The R software (R Core Team, 2023) and RStudio 2024.04.1 (Posit team, 2024) were used to implement both the DRS and DSM models. Similarity between soil properties was assessed using the Wilcoxon rank sum test built in the *stats* package of R Studio (ver. 4.3.1; R Core Team, 2023).

3. Results

3.1. Basic soil properties and spectral characteristics of collected soil samples

Descriptive statistics of soil parameters for the T_{2018}, T_{2021}, and T_{2022} datasets show diverse soil characteristics for the soil samples of the Bundelkhand region (Table 1). Soil textural classes varying from coarse- (loamy sand, sandy loam, and sandy clay loam) to fine-textured (clayey and clay loam) soils, both the T_{2021} and T_{2022} samples are generally more clayey (average clay content > 17.8%) than the T_{2018} samples; the reverse is true for coarse sand. Specifically, T_{2022} samples from Tahrauli show a relatively heavier texture with greater fine sand and clay contents (Table 1). The dominance of heavier textural classes (clay and clay loam) in T_{2022} samples is also evident in the textural triangle (Fig. S3). For all three datasets, several soil samples were slightly alkaline although the EC values were generally low indicating non-saline conditions typical for the region. A critical concern for this region's agricultural productivity is the low to medium SOC content (average SOC: 0.40–0.53%), a finding consistent with other studies on Bundelkhand's degraded soils (Kiran and Kudesia, 2009; Prasad et al., 2020; Ghosh et al., 2021). Average values for the nutrient contents also suggest that these soils are generally deficient in most of the available plant nutrients except for P, Ca, Cu and Mn. For Tahrauli, available P is also low (~2.5 times less than the T_{2018} samples), which is consistent with its high exchangeable Ca contents. Both available Cu and Mn are moderate in their STCR ratings in all three datasets. Moreover, the average values for most soil parameters of the T_{2021} and T_{2022} datasets were significantly (p-value < 0.05) different from those of T_{2018} samples. Specifically, coarse sand and SOC contents, exchangeable K, available S, Zn, B, Fe and Mn contents were lower and the clay content, exchangeable Ca and Mg were higher in both these datasets than those of T_{2018}. Particularly, the average available Zn contents in the T_{2022} samples were about 2 to 3 times less than the T_{2018} and T_{2021} averages. With such differences in soil parameters, the DRS models developed using T_{2018} dataset alone may not be sufficient to quantify the soil parameters of T_{2022} (outside DRS calibration zone) samples supporting the need for spiking T_{2018} dataset with subsamples from T_{2021} and T_{2022} datasets. In contrast, the average values of these three datasets fall within the same STCR rating classes suggesting that the DRS models may perform well in quantifying the STCR ratings required in making nutrient recommendations. With most soil nutrients showing low STCR ratings, there is a pressing need for developing an efficient soil assessment framework for managing soils of smallholder farms in the Bundelkhand region.

Differences in soil properties across three datasets were also seen in the reflectance spectra of soil samples. Results of the principal component (PC) analysis on the processed spectra of T_{2018}, T_{2021} and T_{2022} datasets suggest that the first three PCs could cumulatively explain > 95% of the variance. Resulting biplots using the first 3 PCs along with a convex hull around the T_{2018} data (Islam et al., 2005) in Fig. 3 clearly show that some of the T_{2022} sample data points are outside the spectral space (convex hull) of T_{2018} data. As expected, the T_{2018} and T_{2021} datasets show two distinct patterns in accordance with their distinctive geological origin. The Tahrauli tehsil is located within the Precambrian side close to the boundary between Precambrian rocks and quaternary sediments (Wandrey and Law, 1997) with a few sampling locations having quaternary sediments geology (Fig. 3B and 3C). With a mix of both Precambrian and quaternary sediments geology in the Tahrauli tehsil, a regional-scale DRS model may perform better than a geologic-specific DRS model in the T_{2022} dataset.

3.2. DRS performance within and outside the calibration zones

Purushothaman et al. (2024) showed that spiking of T_{2018} data with 20% of T_{2021} data is needed in developing robust DRS models for soil assessment. Here, we test how such spiked regional-scale SSLs may be used to develop a DRS-DSM pipeline for evaluating soils both within and outside calibration zones. Thus, we calibrated Cubist models in two regional-scale spectral libraries of $RSLS_{in}$ (containing spiking data from within calibration zone) and $RSLS_{out}$ (containing spiking data from outside calibration zone) and tested for estimating soil parameters in the non-spike T_{2021} and T_{2022} (Tahrauli) datasets. Resulting performance statistics (Table 2) suggest that calibrated Cubist models using both the $RSLS_{in}$ and $RSLS_{out}$ datasets performed well for coarse sand and clay contents, exchangeable Ca and Mg with LCCC > 0.7. Specifically,

Table 1
Descriptive statistics of basic soil properties and nutrient contents for samples collected during 2018 (T_{2018}), 2021 (T_{2021}), and 2022 (T_{2022}) datasets of the Bundelkhand region.

Soil parameters	T_{2018}				T_{2021}				T_{2022}			
	Mean	Q1	Q3	CV	Mean	Q1	Q3	CV	Mean	Q1	Q3	CV
Coarse Sand, %	23.9	5.93	45.3	89	**18.0**	3.63	21.1	118	**9.92**	4.37	11.4	87
Fine Sand, %	36.6	27.3	44.4	33	35.9	25.7	46.4	38	35.5	27.5	42.5	32
Clay, %	17.8	8.91	23.2	63	**24.7**	15.3	34.2	47	**30.1**	22.3	38.2	36
pH	7.64	7.20	8.17	9	**7.89**	7.61	8.28	8	**7.82**	7.64	8.05	5
EC, dS/m	0.19	0.11	0.21	78	**0.19**	0.12	0.24	63	**0.11**	0.07	0.13	60
SOC, %	0.53	0.37	0.64	44	**0.40**	0.29	0.46	46	**0.40**	0.31	0.48	35
Av. P	11.0	4.26	14.8	100	12.1	4.48	13.3	111	**4.32**	2.82	4.89	69
Ex. K	152	73.1	201	76	**122**	61.7	155	72	143	110	161	57
Ex. Ca	2332	1254	3092	52	**2999**	1908	4009	45	**4481**	3790	5455	27
Ex. Mg	308	194	388.8	49	**341**	222	441	46	**352**	279	420	32
Av. S	10.2	4.45	10.5	176	**7.85**	3.95	9.12	95	**5.41**	3.69	5.77	61
Av. Zn	0.62	0.30	0.66	152	**0.48**	0.20	0.54	110	**0.18**	0.1	0.22	71
Av. B	0.53	0.34	0.64	50	**0.47**	0.29	0.61	54	**0.44**	0.33	0.52	39
Av. Fe	8.82	3.39	9.69	127	**7.41**	3.28	7.42	128	6.24	4.63	6.59	72
Av. Cu	0.77	0.50	0.92	56	0.77	0.54	0.88	52	0.72	0.58	0.8	29
Av. Mn	10.8	4.92	13.5	84	**7.73**	3.48	9.16	91	**5.76**	3.79	6.8	54
Ex. Na	127	53.0	177	83	130	54.8	173	96	**191**	116	212	70

Q1: first quartile; Q3: third quartile; CV, %: coefficient of variation; SOC: soil organic carbon; EC: electrical conductivity; Av.: available; Ex.: exchangeable; all nutrients are in mg kg^{-1}. Bold font cases indicate the Wilcoxon rank sum test at 5% level of significance.

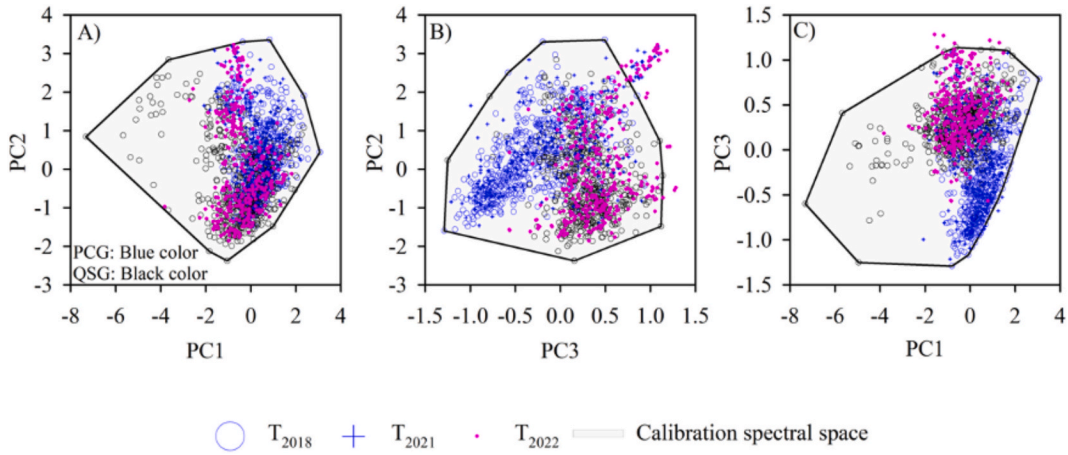

Fig. 3. Convex hull biplots for the T_{2021} and T_{2022} (Tahrauli) spectra overlaid on calibration spectral space of T_{2018} from the Bundelkhand region using standardized principal components (PC). The Precambrian crust geology (PCG) and quaternary sediments geology (QSG) samples were plotted in blue and black color, respectively.

Table 2
Performance statistics of models developed with the regional-scale spectral library spiked with 20% samples collected inside calibration zone during 2021 ($RSLS_{in}$) and $RSLS_{in}$ spiked with 20% samples collected outside calibration zone during 2022 ($RSLS_{out}$) for estimating different soil parameters of the remainder of 2022 samples (Tahrauli tehsil dataset) [Av.: available soil nutrient contents (mg kg^{-1}); Ex.: exchangeable soil nutrient contents (mg kg^{-1}); sand and clay contents are in percentage].

Properties	$RSLS_{in}$					$RSLS_{out}$					Change in performance		*p*-value
	LCCC	RMSE	Bias	PRED(30)	SRA, %	LCCC	RMSE	Bias	PRED(30)	SRA, %	ΔRMSE	ΔSRA	
Coarse sand	0.72	4.89	0.58	43	NA	0.74	4.73	−0.06	46	NA	3	NA	0.30
Fine sand	0.65	7.88	−2.79	88	NA	0.67	7.54	−1.41	87	NA	4	NA	0.56
Clay	0.85	5.40	1.72	83	NA	0.86	5.18	1.12	86	NA	4	NA	0.48
pH	0.57	0.29	0.16	100	99	0.63	0.25	0.06	100	99	14	0	0.04
EC	0.28	0.06	0.05	26	100	0.44	0.05	0.02	43	100	17	0	0
SOC	0.58	0.10	−0.02	77	77	0.63	0.09	0.00	80	77	10	0	0.15
Av. P	0.27	2.66	1.26	39	53	0.43	1.88	−0.19	51	74	29	40	0
Ex. K	0.62	42.9	3.91	70	69	0.64	39.6	2.20	74	68	8	−1	0.18
Ex. Ca	0.88	537	−279	97	86	0.93	418	−95.0	98	90	22	5	0
Ex. Mg	0.72	70.8	10.9	83	81	0.76	62.9	−1.74	88	83	11	2	0.02
Av. S	0.08	6.19	2.53	40	84	0.06	9.00	2.50	43	87	−45	4	0.89
Av. Zn	0.41	0.12	0.08	26	100	0.55	0.09	0.02	48	100	25	0	0
Av. B	0.47	0.12	0.02	69	100	0.52	0.12	0.01	70	100	0	0	0.58
Av. Fe	0.56	2.43	−0.74	51	93	0.66	1.93	−0.49	66	94	21	1	0
Av. Cu	0.60	0.16	−0.03	84	95	0.67	0.14	−0.03	89	96	13	1	0.05
Av. Mn	0.40	2.50	−1.14	49	56	0.49	2.18	−0.67	56	65	13	16	0.02
Ex. Na	0.13	112	−59.9	49	NA	0.25	92.9	−30.1	53	NA	17	NA	0.05

LCCC: Lin's concordance correlation coefficient; RMSE: root-mean-squared error; PRED(30): percentage relative error deviation at 30% error threshold; SRA,%: STCR rating accuracy; ΔRMSE: percentage difference in the RMSE between $RSLS_{in}$ and $RSLS_{out}$ models; ΔSRA: percentage difference in the SRA between $RSLS_{in}$ and $RSLS_{out}$ models; *p*-value: calculated from the absolute error values of $RSLS_{in}$ and $RSLS_{out}$ using the analysis of variance; EC: electrical conductivity (dS m^{-1}); SOC: soil organic carbon (SOC) content (%).

exchangeable Ca showed the highest predictability (LCCC: 0.88–0.93; RMSE: 418–537 mg kg^{-1}) among the soil properties followed by clay contents (LCCC: 0.85–0.86; RMSE: 5.18–5.40%). Most of these soil parameters are spectrally-active soil properties (soil chromophores). Table 2 also shows that spiking a small subset (20%) of T_{2022} samples ($RSLS_{out}$) improved the estimation accuracy of soil properties compared to its counterpart from $RSLS_{in}$ dataset. Specifically, 10 out of 17 soil parameters could be estimated with LCCC > 0.6 when $RSLS_{out}$ was used for calibration as compared to 7 out 17 soil parameters using the $RSLS_{in}$ dataset. This is also reflected in the *p*-values < 0.05 (Table 2) estimated using the analysis of variance (ANOVA) for the absolute error associated with each soil property in the test dataset when two different calibration models were used. Moreover, almost all the soil parameters showed error reduction (ΔRMSE) ranging from 0 to 29%, with the exception of available S. In addition, spiking reduced the bias values while estimating soil properties through the DRS approach compared to the $RSLS_{in}$-calibrated models. Although spiking improves the predictability, some of the nutrient contents such as available P and Mn still showed only low to moderate predictability (LCCC < 0.5); yet, improvements were seen in SRA (ΔSRA) values to the tune of 40% for P and 16% for Mn when models were calibrated using the $RSLS_{in}$ dataset. Out of 17 soil properties, 9 soil parameters showed PRED(30) > 70%, which included some of the micronutrients such as available B and Cu. Moreover, 9 out of 13 soil parameters were well estimated (SRA > 80%); all soil parameters showed SRA values > 70%, except for available Mn using the $RSLS_{out}$-calibrated Cubist model. This improvement in the performance of DRS models in the case of $RSLS_{out}$ data source was also observed from the scatter plots between observed and predicted values (Fig. S4). Close proximity of observed and estimated soil properties along 1:1 line in Fig. S4 particularly for exchangeable Ca and Mg, clay and SOC contents, coarse sand and pH suggests that these parameters are well-predicted when $RSLS_{out}$ is used for calibrating the Cubist models. In general, $RSLS_{out}$ models were unbiased in estimating soil pH, EC, SOC, available P, B and Cu of the non-spike T_{2022} samples. However, available Zn showed an overestimation for most samples (Fig. S4K). Available Zn contents in T_{2022} samples were generally lower than those in the T_{2018}

and T_{2021} datasets. Even the third quartile value of T_{2022} samples is lower than the first quartile value of the T_{2018} dataset (Table 1). Similarly, most of the samples of the T_{2022} dataset were lying below the 1:1 line (Fig. S4L) indicating underestimation of available Mn. Nevertheless, the performance of calibrated models in $RSLS_{out}$ dataset and subsequent testing on non-spike T_{2022} dataset (outside the calibration zone) is similar to those calibrated using $RSLS_{in}$ dataset and tested on non-spike T_{2021} dataset (inside the calibration zone) for most of the soil parameters except for SOC content (Table S4 and Table 2). Results of the PRED(30) and SRA values suggest that the $RSLS_{out}$ models showed a moderate to high prediction level in the non-spike T_{2022} samples. Therefore, the estimates from $RSLS_{out}$ models were used as inputs for developing DRS-based DSM products for the non-spike T_{2022} dataset.

3.3. Digital soil mapping of basic soil properties and nutrient contents

3.3.1. DSM performance within the DRS calibration zone

The non-spike T_{2021} dataset (collected during 2021 from within the DRS calibration zone of 2018) was used to assess the reliability of DRS-estimated soil properties in replacing laboratory-measured properties for DSM. Performance statistics for 17 soil parameters are summarized in Fig. 4 with corresponding RMSE and bias values listed in Table S5. Based on LCCC values, both measured- and DRS-based DSM products showed higher prediction accuracy for coarse sand, fine sand, clay content, pH, available P, Mn, and exchangeable K, Ca, and Mg (LCCC $\geq$ 0.6). Other soil parameters such as available Zn, B, Fe, and exchangeable Na showed moderate predictability (0.4 $\leq$ LCCC $<$ 0.6), while SOC

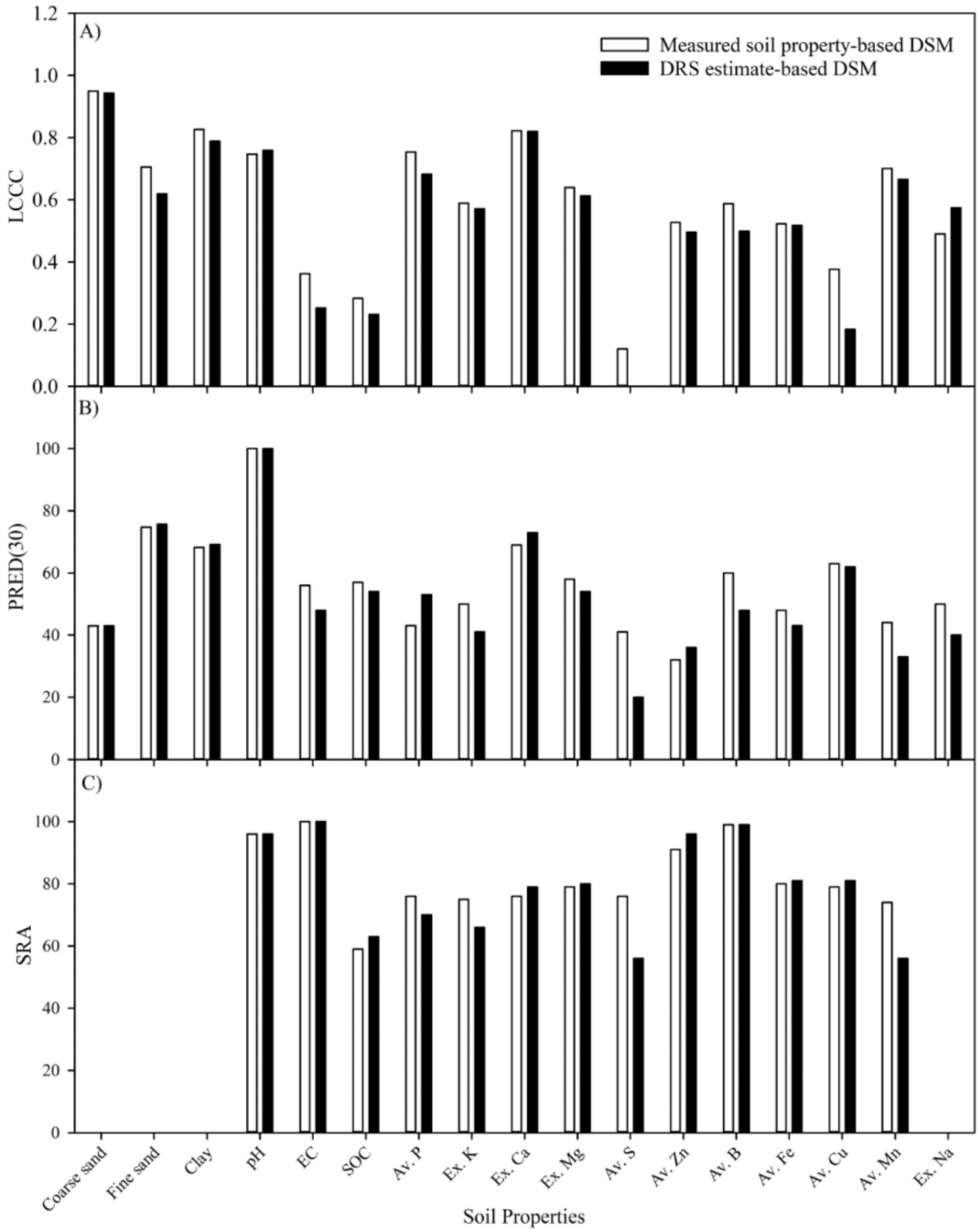

Fig. 4. Bar charts showing Lin's concordance correlation coefficient (LCCC), percentage relative error deviation at 30% error threshold [PRED(30)] and soil test crop response (STCR) rating accuracy (SRA) values for 17 soil parameters tested on non-spike T_{2021} DSM test dataset.

content, EC, and available S showed poor concordance values (LCCC < 0.4). Notably, available Cu showed moderate predictability (LCCC > 0.4) in the measured property-based DSM modelling. However, this trend was not observed in the DRS-based DSM even though the DRS model itself showed good agreement with laboratory-measured Cu (LCCC = 0.73; Table S4). These results indicate that the DRS estimates yield model performance comparable to that from measured values for most soil properties when assessed using LCCC. We also compared the absolute error values for the measured property-based and DRS-based DSM estimates using the ANOVA. No statistically significant (p-values < 0.05) difference was observed between these two approaches for all the soil properties except for available S (p-value = 0.003) suggesting that the estimated DSM products were similar. In contrast, PRED(30) values showed slightly different patterns. The SOC content, available B, and Cu had more than 50% of samples with prediction accuracy above 70% for both measured- and DRS-based DSM products. For other parameters such as available S, Zn, Fe, exchangeable Na, and EC, both measured and DRS-based DSM products showed moderate to low PRED (30) values, consistent with their lower LCCC values. This discrepancy highlights the complementary nature of LCCC and PRED(30). The LCCC evaluates overall concordance between predicted and observed (continuous) values, which accounts for both precision and systematic bias. On the other hand, PRED(30) quantifies the proportion of predictions that fall within an acceptable error threshold. Together, these metrics provide both a statistical and practical perspective on prediction accuracy. Moreover, the qualitative assessment based on the SRA values

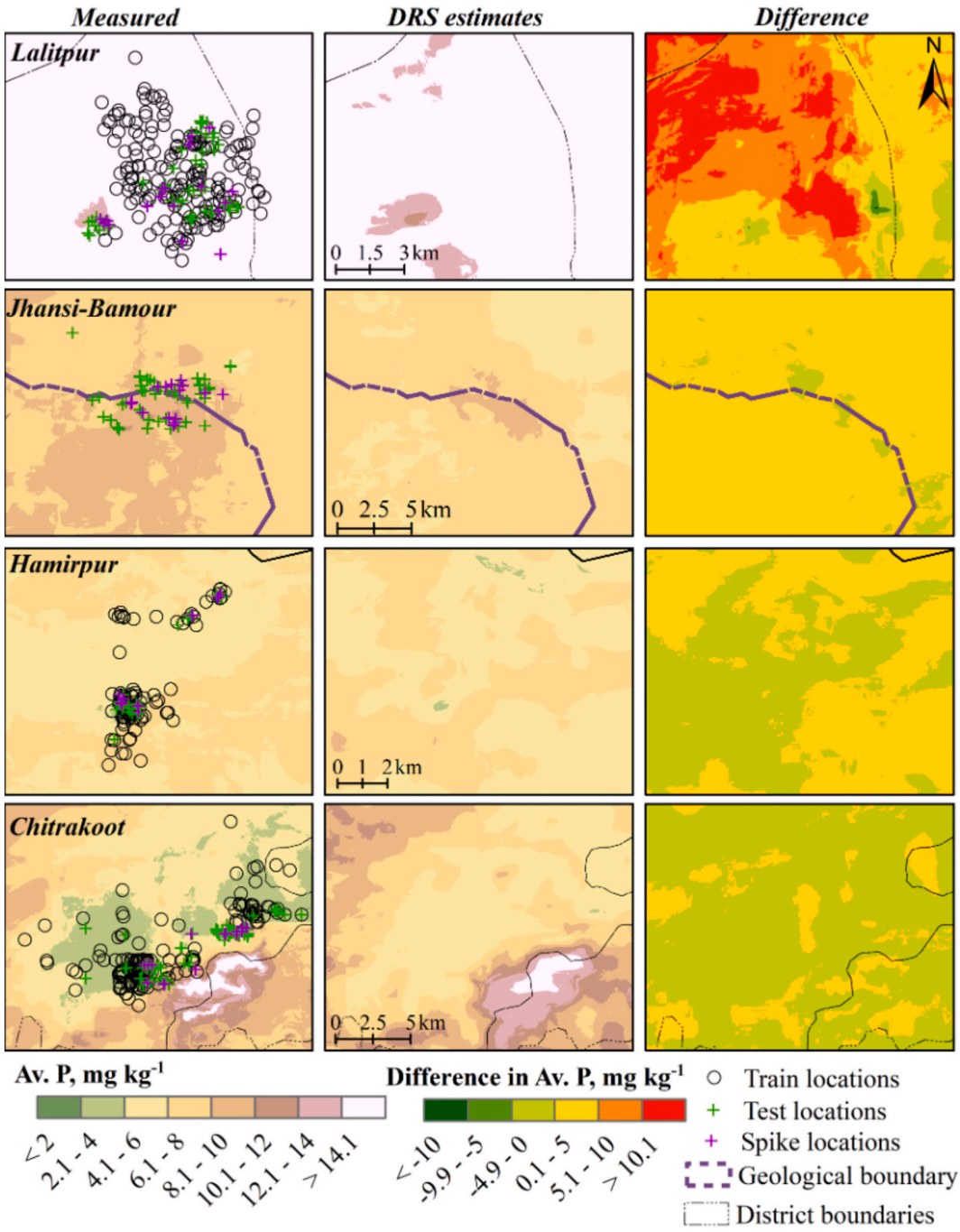

Fig. 5. Digital soil maps developed using measured and diffuse reflectance spectroscopy (DRS)-estimated available P and their difference maps for the selected districts of the Bundelkhand region.

also showed similar results for measured- and DRS-based DSM outputs except for the largest discrepancies observed for available S and Mn. Notably, 9 out of 13 soil parameters showed better estimation accuracy with SRA values > 70% and the soil properties such as SOC content, and exchangeable K showed a moderate performance with SRA value > 60%. Scatter plots between observed vs. predicted soil properties (Fig. S5) further confirmed model performance. Coarse sand, fine sand, clay content, and exchangeable Ca and Mg aligned closely along the 1:1 line, which is indicative of high predictive accuracy. Interestingly, available P estimation using a measured property-based model showed slight overestimation for some samples while DRS-based predictions were better aligned with the 1:1 line and resulting in higher PRED(30) values (Fig. S5-F).

Spatially-continuous maps were generated for all the 17 soil parameters using the trained QRF models from both measured and DRS-estimated soil properties. Available P was selected for detailed discussion due to its direct relevance to crop productivity, nutrient management practices, and regional policy. The measured- and DRS-based DSM maps (Fig. 5) showed broadly consistent spatial patterns with Lalitpur showing higher available P concentrations (>14 mg kg^{-1}). This observation is consistent with previous findings that Precambrian soils contain higher P than Quaternary sediments (Purushothaman et al., 2024). On the other hand, Chitrakoot showed substantial spatial variability (<2 to > 14 mg kg^{-1}) reflecting local soil-forming factors and possibly prevailing management practices. Differences between the two soil mapping approaches were mostly within –5 to + 5 mg kg^{-1} of available P although larger deviations were observed in Lalitpur. Similarly, the 90% prediction interval (PI) maps (Fig. S6) of Lalitpur also showed higher PI values compared to the other districts. Moreover, the 90% PI values from DRS-based DSM are smaller than those from measured property-based DSM products suggesting that the 5% and 95% PI values in the DRS-based DSM are very close to each other (narrow uncertainty bounds) than the DSM based on measured soil properties. The 90% PI uncertainty maps suggest that error propagation from DRS did not amplify uncertainty, and, in some cases, may have smoothed local variability consistent with the findings of Chen et al. (2023). Similarly, The STCR classification maps (Fig. S7) also showed high agreement with minor misclassifications confined to Chitrakoot.

3.3.2. DSM performance outside the DRS calibration zone

DSM performance was evaluated using the T_{2022} non-spike dataset, which represents samples outside the original DRS calibration zone. Here, DRS-estimated soil properties were obtained using the $RSLS_{out}$ models (developed with the T_{2022} spiked subset), while measured soil properties provided a benchmark for comparison. This framework enabled a direct evaluation of how transferring DRS models beyond their original calibration zone influences subsequent DSM accuracy. The performance statistics for both measured- and DRS-based DSM models are summarized in Table 3. Among all soil parameters, exchangeable Ca showed better predictability (LCCC > 0.53) for both measured- and DRS-based models, while other properties generally showed low to moderate concordance values. However, the PRED(30) metric indicated that measured property-based DSM achieved prediction accuracies above 70% in > 70% of samples for 11 out of 17 parameters. In contrast, six parameters met this threshold for the DRS-based DSM. These results suggest that even when continuous agreement metrics (LCCC) are moderate, the majority of samples are still predicted with acceptable accuracy. Moreover, the differences in PRED(30) values between measured- and DRS-based DSM were less than 5% for most soil parameters. Results of the ANOVA on absolute errors for measured property-based and DRS-based DSM products also showed no significant difference (p-value < 0.05) for most of the soil properties except for SOC content (p-value < 0.049) and available S (p-value < 0.001). In fact, the SOC content, EC, available S, and Fe showed 10–20% fewer samples predicted with < 30% error in the DRS-based models compared to its measured soil property-based DSM products (Table 3). Despite low quantitative performance, the qualitative analysis based on the SRA metric indicated reasonable DSM reliability. The SRA values exceeded 70% for 11 out of 13 parameters in both approaches and their differences were < 7% except for SOC. Observed versus predicted plots (Fig. S8) confirmed strong alignment along the 1:1 line for clay, pH, and exchangeable Ca and Mg. However, some micronutrients were slightly underestimated in the DRS-based DSM showing relatively high bias values.

Using these trained QRF models, spatially-continuous soil property maps for 17 soil parameters were generated for both measured- and DRS-estimated soil properties. Following the DSM testing on the T_{2021} dataset (within the DRS calibration zone), the available P was selected for detailed discussion. The available P estimation and STCR class maps are shown in Fig. 6 and corresponding 90% PI maps are shown in Fig. S9. Overall, the available P content is generally low (<5 mg kg^{-1}) across the study area except for a small patch in the north-western part of Tahrauli. This highlights the need for improving P nutrition in selected smallholder farms in a large section of the Tahrauli tehsil. Both measured- and DRS-based DSM approaches provided broadly similar estimations of available P with differences ranging from –2.9 to 3.9 mg kg^{-1}.

Table 3
Performance statistics for the digital soil mapping (DSM) approach using measured soil data and those estimated using the diffuse reflectance spectroscopy (DRS) approaches in the test datasets created from non-spike samples collected during 2022 (outside primary calibration zone).

Soil properties	DSM using measured soil data					DSM using DRS-estimated soil data					Difference in performance	
	LCCC	RMSE	Bias	PRED(30)	SRA	LCCC	RMSE	Bias	PRED(30)	SRA	$PRED(30)_{diff}$	SRA_{diff}
Coarse sand, %	0.26	6.35	1.06	31	NA	0.17	6.44	0.97	28	NA	3	NA
Fine sand, %	0.35	9.09	−1.31	80	NA	0.30	9.32	−2.22	76	NA	4	NA
Clay content, %	0.42	8.28	0.08	72	NA	0.34	8.86	1.23	70	NA	2	NA
pH	0.40	0.26	−0.02	100	100	0.29	0.25	0.04	100	100	0	0
EC, dS m^{-1}	0.27	0.05	−0.01	69	100	0.15	0.05	0.01	49	100	20	0
SOC content, %	0.47	0.11	−0.02	78	69	0.01	0.14	−0.02	65	54	13	15
Av. P, mg kg^{-1}	0.14	1.89	−0.17	59	70	0.10	1.94	−0.39	58	77	1	−7
Ex. K, mg kg^{-1}	0.27	41.6	−5.77	72	57	0.21	43.7	−8.06	68	58	4	−1
Ex. Ca, mg kg^{-1}	0.53	783	−66.4	89	84	0.56	779	−156	92	81	−3	3
Ex. Mg, mg kg^{-1}	0.26	96.7	−11.0	78	73	0.15	99.3	−13.1	77	72	1	1
Av. S, mg kg^{-1}	−0.03	1.91	−0.09	59	99	−0.11	4.21	1.90	45	92	14	7
Av. Zn, mg kg^{-1}	0.28	0.08	0.00	53	100	0.17	0.09	0.02	50	100	3	0
Av. B, mg kg^{-1}	0.21	0.13	−0.02	72	100	0.08	0.14	−0.01	68	100	4	0
Av. Fe, mg kg^{-1}	0.29	1.65	0.32	72	97	0.02	1.98	−0.33	59	97	13	0
Av. Cu, mg kg^{-1}	0.32	0.16	0.00	86	97	0.14	0.17	−0.02	86	97	0	0
Av. Mn, mg kg^{-1}	0.38	1.94	0.09	70	72	0.12	2.15	−0.65	65	70	5	2
Ex. Na, mg kg^{-1}	0.21	84.2	−0.36	59	NA	0.09	89.3	−31.3	59	NA	0	NA

LCCC: Lin's concordance correlation coefficient; RMSE: root-mean-squared error; PRED(30): percentage relative error deviation at 30% error threshold; SRA,%: STCR rating accuracy; EC: electrical conductivity; SOC: soil organic carbon; Av.: available soil nutrient contents; Ex.: exchangeable soil nutrient contents.

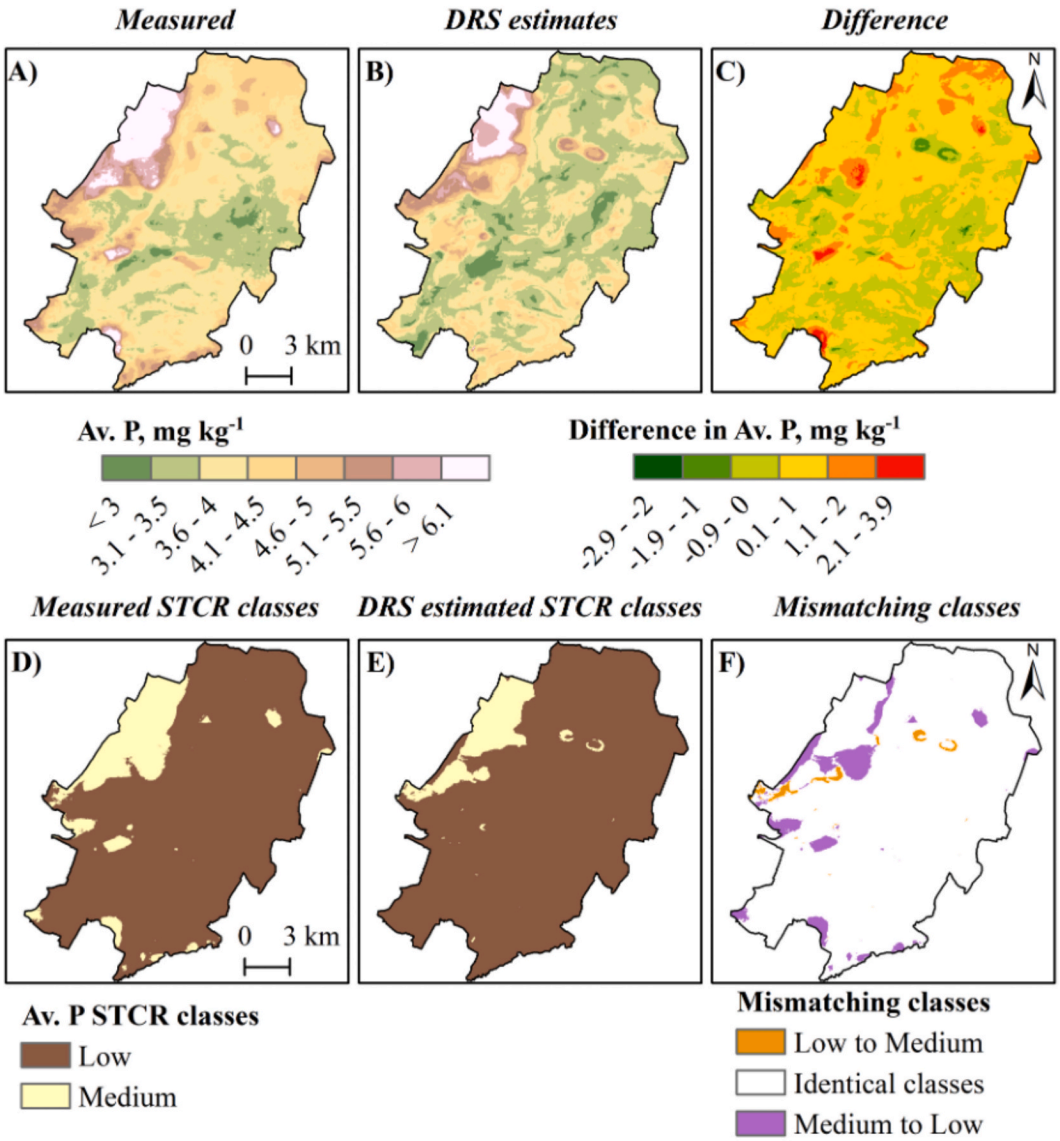

Fig. 6. Digital soil maps created using laboratory-measured and diffuse reflectance spectroscopy (DRS)-estimated available P and their corresponding STCR rating classes map for the Tahrauli dataset collected during 2022.

Corresponding STCR class maps showed largely identical classifications, with only minor mismatches where the DRS-based DSM slightly underestimated available P. Similarly, the 90% PI maps showed that prediction uncertainties for the majority of pixels remained below 5 mg kg^{-1}.

3.4. Influence of DRS estimation accuracy on DSM predictions

The PRED(30) was used to evaluate the effect of using DRS-estimated soil properties instead of measured values for DSM. Fig. 7 shows bar charts of PRED(30) values in the non-spike DSM test datasets of T_{2021} (within the DRS calibration zone) and T_{2022} (outside the DRS calibration zone) using DRS alone, and both measured- and DRS-based DSM approaches. In general, the DRS-based DSM approach produced PRED(30) values comparable to or slightly lower than those obtained using measured soil property-based DSM in both T_{2021} and T_{2022} test datasets. The differences in PRED(30) values between measured- and DRS-based DSM products ranged from −8% to 21% for T_{2021} and −3% to 20% for T_{2022} (Table 3). Specifically, soil EC and available S showed > 10% fewer well-predicted samples (<30% error) in the DRS-based DSM compared to their measured counterparts in both datasets. This may be attributed to their weak spectral signatures, which reduced the accuracy of their DRS predictions. In T_{2021}, available B and Mn showed a 10–11% reduction in accurately-predicted samples in the DRS-based DSM compared to the measured soil property-based DSM estimates. Similarly, the SOC content and available Fe in the T_{2022} test dataset showed a 12–14% reduction in predictability. Despite these exceptions, most other properties showed comparable accuracy between the two DSM approaches in both datasets. Interestingly, several nutrients such as available P, S, Zn, Fe, Cu, Mn, and exchangeable Na in the T_{2022} test dataset showed better predictability in the DSM approach (irrespective of measured or DRS estimated soil properties as inputs for DSM modelling) compared to the DRS-only models. This suggests that these nutrients are highly influenced by the local-scale environmental conditions; the spectral data alone fails to capture these environmental effects in the chemometric modelling.

We also observed that the difference between the PRED(30) values of different soil parameters obtained through DSM modelling using measured soil properties and those estimated using DRS approach exponentially decreased as the PRED(30) values for the DRS-estimated

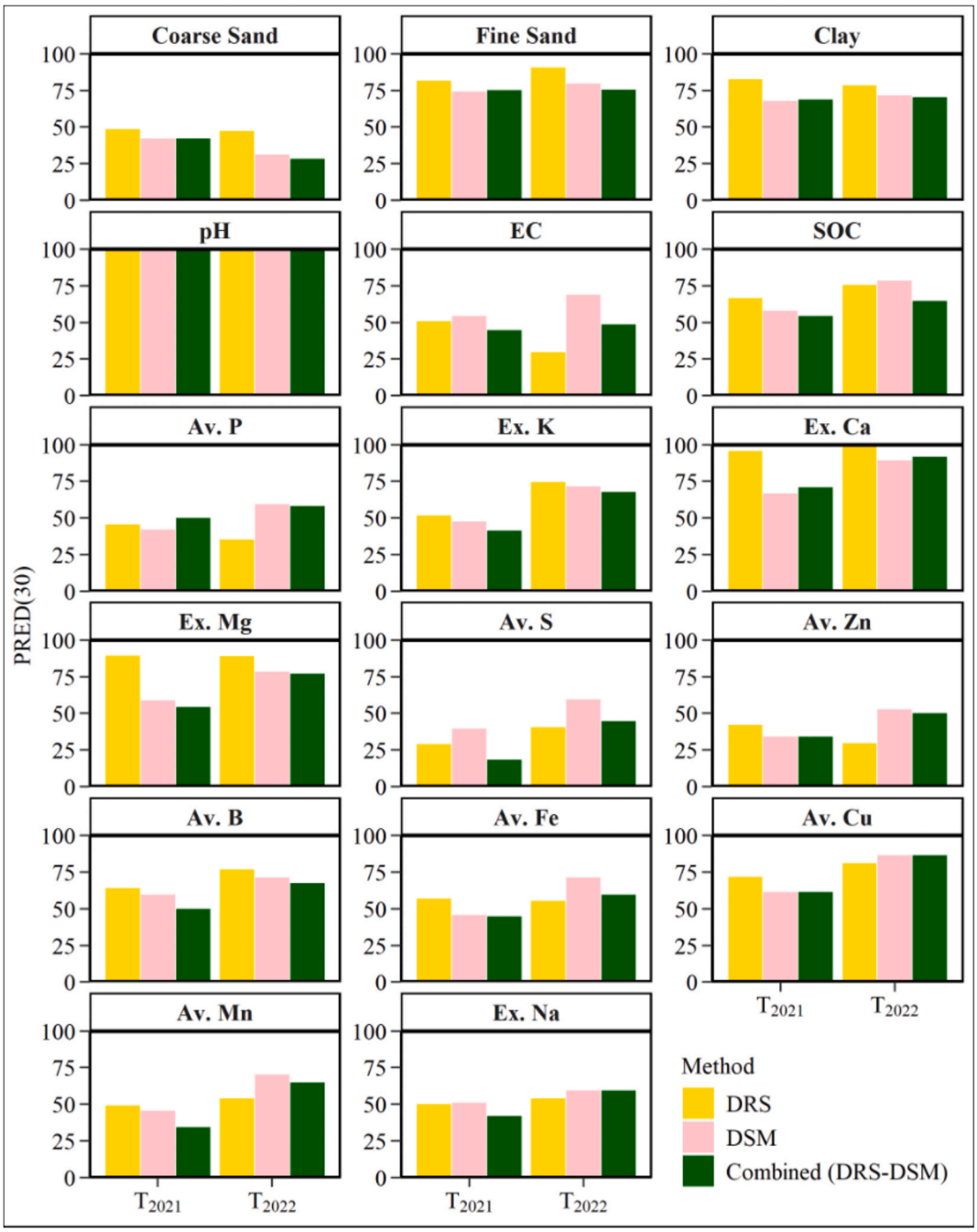

Fig. 7. Percentage relative error deviation (PRED) at 30% error threshold for the non-spike T_{2021} and T_{2022} datasets developed using the diffuse reflectance spectroscopy (DRS), digital soil mapping (DSM), and combined DRS and DSM approaches.

soil properties increased (Fig. 8). This suggests that well-performing DRS models (high PRED values) have the potential to match or even surpass traditional DSM approaches where measured soil properties are used for geospatial mapping. For instance, exchangeable Ca was predicted very accurately by the DRS approach with PRED(30) values > 96% in both T_{2021} and T_{2022} non-spike datasets. When these estimates were used in the DSM framework, the proportion of well-predicted samples further increased by about 3–4% compared to the measured property-based DSM. Such a result demonstrates the added value of combining spectral information with environmental covariates, particularly, for properties with strong spectral signatures. Broadly, they underscore the importance of improving the robustness of DRS approach so that spectral estimates can reliably complement or, in some cases, substitute conventional wet chemistry-based soil properties in the DSM workflows.

4. Discussion

4.1. Spatio-temporal transferability of DRS models

The multi-year Bundelkhand dataset allowed testing of calibrated DRS models on spatially- and temporally-independent samples from smallholder farms distributed over a large area with contrasting geological origin. The T_{2018} samples covering the sedimentary and Precambrian lithology of 8 Bundelkhand district were used to form a regional SSL, which served as a primary calibration dataset. The Cubist models trained with the T_{2018} dataset were tested on a) T_{2021} dataset collected from the same region after 3 years of implementing land

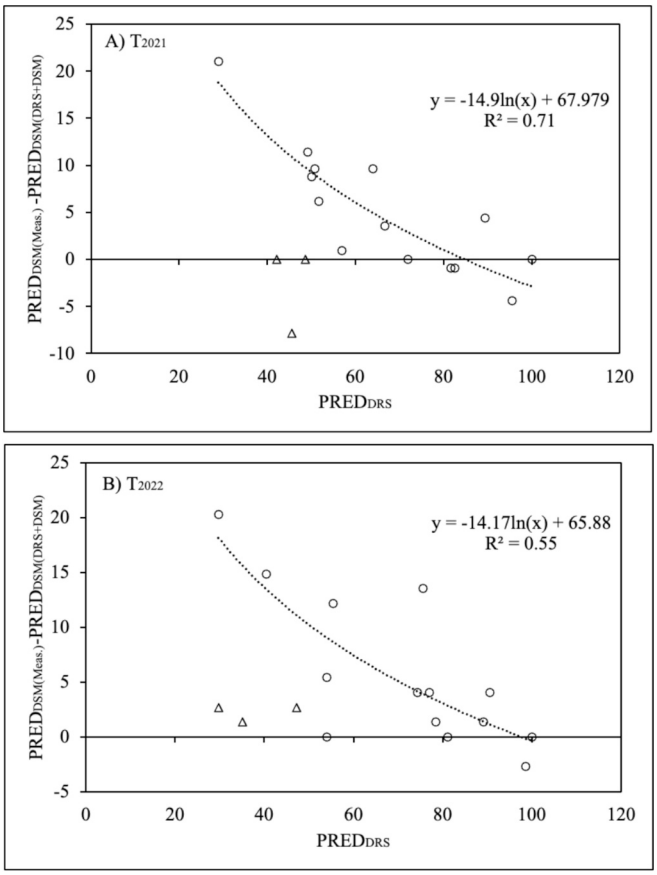

Fig. 8. Scatter plot between the difference in soil properties estimated using the diffuse reflectance spectroscopy (DRS) approach and the combined DRS and digital soil mapping (DSM) approaches vs. percentage relative error deviation at 30% error threshold [PRED(30)]. Triangles represent values obtained for the coarse sand content, available P and Zn; the remainder of the parameters are shown using circles.

development measures and b) T_{2022} dataset compiled from altogether a new site with no prior samples collected during 2018 or 2021. The T_{2021} served as a temporally-independent test dataset and T_{2022} served as both temporally- and spatially-independent test dataset. Earlier, Purushothaman et al. (2024) showed that spiking the T_{2018} data using 20% of the T_{2021} data improved the performance of resulting Cubist models as was also reported by Luce et al. (2022). Model transferability of calibrated models with such a spiked $RSLS_{in}$ (T_{2018} + 20% of T_{2021} as spiking samples) from within the calibration zone, however, was limited when tested on the dataset outside the calibration zone (i.e., non-spike data of T_{2022}). Specifically, only 7 out of 17 soil properties were predicted with LCCC > 0.6 reflecting limited transferability of temporally-spiked DRS models outside their calibration zones. Addition of the 20% of T_{2022} samples to the $RSLS_{in}$ dataset (i.e., both spatially- and temporally-spiked $RSLS_{out}$ dataset) improved predictions to 10 out of 17 properties in the non-spike T_{2022} dataset, consistent with previous studies showing that spiking enhances DRS model accuracy (Shepherd and Walsh, 2002; Ng et al., 2022; Zayani et al., 2023) even beyond the calibration zone. Moreover, spiking reduced model bias and improved stability. Compared to un-spiked models, the spiked DRS models showed lower bias for pH, SOC, Ca, Mg, and micronutrients producing robust and less site-dependent predictions. Although spiking the primary calibration dataset of T_{2018} using subsets of T_{2021} and/or T_{2022} datasets weakens the spatial and temporal independence of test datasets, it is a necessary step to expand the spectral space (Fig. 3) of calibration data for improving the estimation accuracies of DRS models in test samples. Thus, the spiked DRS models become transferable across spatial and spatio-temporal scales because of the inclusion of variability of new (future) samples within the spectral space of the calibration samples. Ability to estimate multiple soil parameters using spiked DRS models provide a foundation for using DRS-estimated soil properties as inputs in DSM models for creating spatially-continuous soil property maps for both within and outside the calibration zones of the augmented DRS models.

4.2. Performance of DRS-DSM pipeline for soil testing in smallholder farms

The DRS-DSM modelling pipeline was tested by substituting measured soil properties with the DRS-estimated ones as inputs in the QRF model for generating DSM products. Results suggest that DSM models trained on measured and DRS-estimated soil properties performed comparably within the DRS calibration zone. Specifically, soil textural fractions, pH, and exchangeable Ca and Mg consistently showed high predictability reflecting their strong dependence on stable covariates such as topography, parent material, and climate (McBratney et al., 2003; Mulder et al., 2016; Ma et al., 2019; Chen et al., 2022). The geological contrast between Precambrian formations and Quaternary sediments in the study area further reinforced these patterns. In contrast, the SOC content, EC, and available S were poorly predicted, even when measured values were used as inputs. The dynamic nature of SOC, its sensitivity to management, and its weak coupling with static covariates constrain its predictability at regional scales (Stockmann et al., 2015; Padarian et al., 2022). The estimation accuracies for DSM-based SOC contents of this study were consistent with previous studies (Padarian et al., 2017; Reddy et al., 2021; Wang et al., 2022).

Although the T_{2021} DSM models based on measured or DRS estimated soil properties achieved relatively high prediction accuracy for stable soil parameters within the DRS calibration zone, their performance reduced when applied to T_{2022} dataset (i.e., outside the DRS calibration data). Out of 17 soil parameters, only 7 soil parameters showed PRED (30) values > 0.7 in DRS-based DSM approach when tested on the T_{2022} dataset (outside calibration zone samples). Moreover, the DSM modelling efficiencies were also low even when measured properties were used as inputs in the QRF models. This may be because of the smaller number of training samples in the T_{2022} dataset. For the DRS-based DSM, an additional reduction occurred because soil property estimates were derived from models applied outside their primary calibration domain, making them less reliable than measured inputs. Interestingly, the estimated error values for the DSM products captured with LCCC and PRED(30) values were similar when the DRS-estimated soil properties replaced their measured counterparts through conventional wet chemistry approaches validating the operational replacement potential of DRS-estimated soil properties for rapid DSM. Moreover, the DRS-based DSM products captured major spatial patterns in basic soil properties and key nutrient distributions despite some of the cases with reduced DSM modelling accuracy. Spatial consistency between DRS- and measured-based DSM maps (e.g., available P and Ca distributions) confirmed that the pipeline captures real soil–landscape processes even outside calibration zones.

Another significant result of the DRS-DSM pipeline is the high classification accuracy achieved with the DSM-estimated soil properties. Specifically, the STCR ratings extracted for 13 soil parameters measured at different sampling locations matched well with those obtained from both measured property-based DSM and DRS-DSM pipeline (Table 3). In fact, 9 out of 13 nutrient parameters estimated through the DRS-DSM pipeline achieved > 70% STCR rating accuracy. Comparable SRA values for both these DSM products suggests that the STCR-based nutrient recommendations can safely be implemented using the DRS-based DSM. This demonstrates that even with inputs from outside the original calibration zone, DRS-based DSM can provide reliable guidance for nutrient management, particularly, in smallholder farms with resource-limited settings.

Prediction accuracy of the DSM approach primarily depends on the spatial structure of the target soil property and its relationship with environmental covariates. The DSM approach is known to depend on multiple sources of uncertainty including positional, analytical, covariate, and model errors (Grimm and Behrens, 2010; Nelson et al., 2011; Heuvelink, 2018). Moreover, not all soil properties have covariates that directly serve as a soil-forming factor; in fact, several indirect and/or multi-factor relationships and local geomorphic processes can create variability in soil properties even under similar conditions (Behrens et al., 2010; Ma et al., 2019). Similarly, the DRS approach also has its inherent limitations of weak spectral signatures over the VNIR region. Moreover, many of the soil parameters estimated in the DRS approach are known to be soil non-chromophores (Sarathjith et al., 2014). Nevertheless, the similarity in the STCR ratings observed with the DRS-DSM pipeline in outside calibration zone samples provides a significant evidence for utilizing such a technology combination for making nutrient recommendations in every smallholder farm of a targeted region.

4.3. *Error propagation in DRS-DSM pipeline for soil testing in smallholder farms*

Because DRS-estimated soil properties carry both measurement and modelling uncertainties, it is important to evaluate how these errors propagate into the DSM predictions. In practice, DSM studies often propagate input errors using linear approximations or simulations, such as first-order Taylor series expansions (Heuvelink et al.,1989; Dobarco et al., 2019) or Monte Carlo methods (Bishop et al., 2006; Brodský et al., 2013, Heuvelink, 2018). In our study, formal error-propagation methods were not feasible because DRS models were developed using the Cubist model, which does not provide straightforward variance estimation. Instead, we adopted the PRED(30) metric which quantifies the proportion of samples predicted with less than 30% relative error. The PRED (30) allowed us to assess how error in DRS models translated into a reduced percentage of well-predicted samples in DSM outputs. Soil properties with weak spectral responses (e.g., EC, available S, B, Mn) showed 10–20% fewer samples predicted with $<$ 30% error in DRS-based DSM compared to measured property-based DSM. For SOC content and available Fe, reductions in the order of 12–14% were observed in the T_{2022} dataset (outside the DRS calibration zone). Conversely, soil properties with strong spectral signatures (i.e., exchangeable Ca) achieved PRED(30) values $>$ 96% in DRS-only models and even showed a slight increase in the proportion of well-predicted samples when used in the DRS-based DSM illustrating the potential of strong DRS models to enhance DSM accuracy. This may also be observed from Fig. 9, which shows covariates structures for two scenarios using a well-predicted soil property such as exchangeable Ca and poorly-predicted SOC content for outside the DRS calibration zone. The increasing order of the mean importance values in this figure suggests that both the specific covariates and their number within each category (climate, terrain and vegetation) more or less remain the same for well-predicted soil properties such as exchangeable Ca (Fig. 9C). However, this structure changed when the estimation accuracies differed. For the SOC contents, the climate variables were not selected for the DRS-based DSM

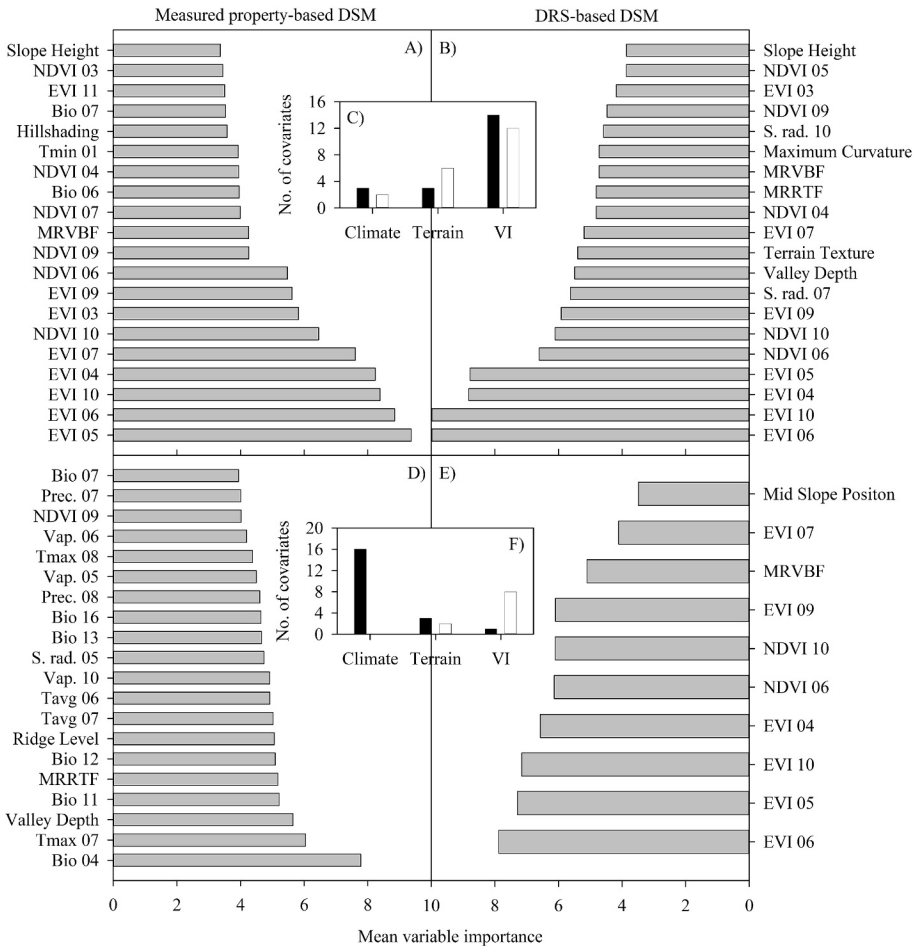

Fig. 9. Top 20 Boruta-selected covariates for the exchangeable Ca (A – C) and soil organic carbon (SOC) contents (D-F) for the laboratory measured property-based and diffuse reflectance spectroscopy (DRS)-based digital soil mapping (DSM) approaches. The bar chart shows the number of covariates within a specific category for measured property-based (black bar) and DRS estimates-based (unfilled bar) DSM approaches.

modelling while more vegetation indices were selected compared to measured SOC-based DSM (Fig. 9F). Similar results were also seen for the available S and Fe, which showed reduced estimation accuracy when their DRS estimates were used as inputs in DSM modelling. Hence, the DRS predictability had a greater influence in shifting the covariate structure, which indirectly influenced the DSM performance.

Overall, reductions in well-predicted samples followed a logarithmic trend with baseline DRS model accuracy (Fig. 8). This indicates that better DRS models can help DSM achieve prediction performance similar to or higher than measured property-based DSM. Even when reductions occurred, environmental covariates in the DSM framework helped buffer weaknesses in DRS estimates by capturing pedogenic processes not directly represented in spectral data. These findings highlight both the potential and limitations of integrating DRS estimates into DSM: the approach is scalable and cost-effective and provides comparable performance to laboratory-based DSM for many soil properties although its effectiveness depends on the spectral predictability of the target property. Yet, some limitations still remain unresolved. The use of downscaled covariates (e.g., 1 km climate data resampled to 10 m) may have introduced spatial scale mismatches. With > 85% of agricultural fields in India are small and marginal farms (Das et al., 2022), the scale mismatch in the climatic covariates remains a primary challenge for implementing DRS-DSM pipeline in smallholder farms. The absence of management information (e.g., tillage, cropping, fertilization history) and the relatively small outside calibration zone SSL also constrained model performance. Future research should expand calibration datasets, integrate management data, and perform rigorous uncertainty analyses. Advances in deep learning and multisource data fusion, such as combining DRS with hyperspectral or multispectral imagery may offer opportunities to improve the accuracy and generalizability of the DRS-DSM pipeline.

4.4. Implementing DRS technology in smallholder farms

Transferring DRS models across time and space remains a critical bottleneck for operationalizing soil spectroscopy and its subsequent use for building a DRS-DSM pipeline. With multi-year Bundelkhand dataset, we showed that while temporal changes (e.g., land development measures between T_{2018} and T_{2021}) introduce spectral variability, spatial heterogeneity presents a significantly harder barrier to model generalization. It is also observed that spiking the baseline model (T_{2018}) with temporal samples (T_{2021}) successfully corrected for temporal drift within the same region. However, this "temporally-corrected" model failed to generalize to the spatially-independent T_{2022} site data (yielding LCCC > 0.6 for only 7 of 17 properties). This suggests that the spectral variance introduced by changing geographical locations (and potentially underlying parent material or texture classes) exceeds the variance captured by simply updating the model with recent samples from the original location. The model was essentially "over-fitted" to the spectral characteristics of the calibration zone regardless of the time of sampling. The significant improvement in prediction accuracy (10 of 17 properties) achieved by adding a subset of T_{2022} samples to the calibration set confirms the efficacy of spiking for correcting spatial bias. Consistent with findings by Shepherd and Walsh 2002 and Zayani et al. (2023), we also found that expanding the global calibration dataset with adequate local representation is crucial. This process effectively expands the spectral domain (Fig. 3), forcing the Cubist algorithm to generate rules that encompass the specific soil-attribute relationships of the new site. It is important to acknowledge that spiking the primary calibration dataset (T_{2018}) with subsets of test datasets (T_{2021} or T_{2022}) technically weakens the strict statistical independence of the validation. However, we argue that this trade-off is justifiable and necessary for the practical deployment of DRS. In a precision agriculture context, the goal is not merely to validate a static historical model, but to deploy a dynamic, evolving spectral library. Our results indicate that a "living" spectral library, which ingests a small number of samples from new sites to recalibrate itself is the only viable pathway for maintaining high estimation accuracies across large, heterogeneous landscapes such as Bundelkhand. This "living" spectral library approach effectively reduces analytical costs while improving site-specific predictions. The cost of analyzing 20% of samples via wet chemistry to calibrate and to predict the remaining 80% via DRS is a fraction of the cost required for a full laboratory campaign. This efficiency allows for the increased sample point density required for high-resolution DSM, which is essential for identifying SOC hotspots or nutrient deficiencies at the field scale.

5. Conclusion

The primary goal of this study was to evaluate the utility of a combined DRS-DSM modelling pipeline for estimating soil properties in every smallholder farm of a large region. Using multi-year datasets from smallholder farms in the Bundelkhand region, we assessed the transferability of DRS models, tested the benefits of spiking strategies, and examined how DRS-derived estimates can support reliable DSM modelling such that the DRS-DSM pipeline meets the needs of general soil testing and nutrient management in particular. The transferability of DRS models to test soil samples originating both from the calibration zone and outside the calibration zone was tested using spiked spectral datasets and Cubist models. Results showed that the spiked models with spiking data from within the calibration zone ($RSLS_{in}$) performed well in estimating soil properties in the test samples collected within the same region. However, the $RSLS_{in}$ model predicted only 7 out of 17 properties with LCCC > 0.6 when applied to soil samples collected from outside the calibration zone (T_{2022}). Spiking the $RSLS_{in}$ dataset with 20% of the T_{2022} samples ($RSLS_{out}$) improved model performance allowing 10 out of 17 properties to achieve LCCC > 0.6 and reducing prediction errors by 3——29%. More importantly, spiking the $RSLS_{in}$ data with samples from outside the calibration zone could improve the STCR classification accuracy with SRA values exceeding over 70% for most parameters demonstrating that spiking effectively captures local variability even when test data originates from entirely outside the calibration zones. The results of DSM approaches showed that the both measured and DRS-estimated soil properties may be used as inputs for generating DSM products with comparable performance within the DRS calibration zone. However, DRS-based DSM products were observed to be less reliable for the region outside the main calibration zone possibly because of limited sample size. Nevertheless, several key soil properties such as fine sand, clay, pH, exchangeable Ca, Mg, and available Cu still achieved high accuracy with PRED(30) values in the range of 70——100%. Moreover, 11 out of 13 soil parameters showed the SRA values > 70% for DRS-based DSM approach in the T_{2022} dataset. Specifically, our results showed that the DRS-based DSM products generally showed narrower uncertainty ranges which highlights the robustness of the approach. The current study provides evidence that DRS approaches, if suitably spiked and calibrated, may be used for soil testing both within and outside the calibration zones within a given region. Thus, the DRS-DSM pipeline provides a cost-effective and reliable complement to conventional wet chemistry for making soil management decisions.

CRediT authorship contribution statement

Naveen K. Purushothaman: Writing – original draft, Visualization, Validation, Software, Data curation, Conceptualization. **Kaushal K. Garg:** Writing – review & editing, Project administration, Investigation. **Nagaraju Budama:** Formal analysis. **Venkataradha Akuraju:** Writing – review & editing, Resources, Project administration. **K.H. Anantha:** Writing – review & editing, Resources, Project administration. **Ramesh Singh:** Project administration, Funding acquisition. **M.L. Jat:** Writing – review & editing, Resources, Project administration. **Bhabani S. Das:** Conceptualization, overall supervision, drafting of original manuscript and editing.

Declaration of competing interest

The authors declare that they have no known competing financial interests or personal relationships that could have appeared to influence the work reported in this paper.

Acknowledgement

The first author acknowledges the Prime Minister's Research Fellowship (PMRF), Round 10 (lateral entry) for his PhD research. We thank the Government of Uttar Pradesh for providing financial assistance to implement a range of drought mitigation and productivity enhancement interventions in the Tahrauli cluster under RKVY (Rashtriya Krishi Vikas Yojana) during 2022–2025. We also acknowledge the CGIAR Mega Program (NEXUS Gains and Multifunctional Landscapes) for partially supporting the time of ICRISAT scientists.

Appendix A. Supplementary data

Supplementary data to this article can be found online at https://doi.org/10.1016/j.geoderma.2026.117749.

Data availability

The authors do not have permission to share data.

References

Barnes, R.J., Dhanoa, M.S., Lister, S.J., 1989. Standard normal variate transformation and de-trending of near-infrared diffuse reflectance spectra. Appl. Spectrosc. 43 (5), 772–777.
Behrens, T., Schmidt, K., MacMillan, R.A., Viscarra Rossel, R.A., 2018. Multi-scale digital soil mapping with deep learning. Sci. Rep. 8 (1), 15244.
Behrens, T., Schmidt, K., Zhu, A.X., Scholten, T., 2010. The ConMap approach for terrain-based digital soil mapping. Eur. J. Soil Sci. 61 (1), 133–143.
Bishop, T.F., Minasny, B., McBratney, A.B., 2006. Uncertainty analysis for soil-terrain models. Int. J. Geogr. Inf. Sci. 20 (2), 117–134.
Brodský, L., Vašát, R., Klement, A., Zádorová, T., Jakšík, O., 2013. Uncertainty propagation in VNIR reflectance spectroscopy soil organic carbon mapping. Geoderma 199, 54–63.
Brunet, D., Barthès, B.G., Chotte, J.L., Feller, C., 2007. Determination of carbon and nitrogen contents in Alfisols, Oxisols and Ultisols from Africa and Brazil using NIRS analysis: effects of sample grinding and set heterogeneity. Geoderma 139 (1–2), 106–117.
Chen, S., Arrouays, D., Mulder, V.L., Poggio, L., Minasny, B., Roudier, P., Libohova, Z., Lagacherie, P., Shi, Z., Hannam, J., Meersmans, J., 2022. Digital mapping of GlobalSoilMap soil properties at a broad scale: a review. Geoderma 409, 115567.
Chen, S., Saby, N.P., Martin, M.P., Barthes, B.G., Gomez, C., Shi, Z., Arrouays, D., 2023. Integrating additional spectroscopically inferred soil data improves the accuracy of digital soil mapping. Geoderma 433, 116467.
Dai, L., Wang, Z., Zhuo, Z., Ma, Y., Shi, Z. and Chen, S., 2025. Prediction of soil organic carbon fractions in tropical cropland using a regional visible and near-infrared spectral library and machine learning. Soil and Tillage Research, 245, p.106297.
Dalal, R.C. and Henry, R.J., 1986. Simultaneous determination of moisture, organic carbon, and total nitrogen by near infrared reflectance spectrophotometry. Soil Science Society of America Journal, 50(1), pp.120-123.
Das, B.S., Sarathjith, M.C., Santra, P., Sahoo, R.N., Srivastava, R., Routray, A., Ray, S.S., 2015. Hyperspectral remote sensing: opportunities, status and challenges for rapid soil assessment in India. Curr. Sci. 860–868.
Das, B.S., Wani, S.P., Benbi, D.K., Muddu, S., Bhattacharyya, T., Mandal, B., Santra, P., Chakraborty, D., Bhattacharyya, R., Basak, N., Reddy, N.N., 2022. Soil health and its relationship with food security and human health to meet the sustainable development goals in India. Soil Secur. 8, 100071.
Dobarco, M.R., Bourennane, H., Arrouays, D., Saby, N.P., Cousin, I., Martin, M.P., 2019. Uncertainty assessment of GlobalSoilMap soil available water capacity products: a French case study. Geoderma 344, 14–30.
Fick, S.E., Hijmans, R.J., 2017. WorldClim 2: new 1-km spatial resolution climate surfaces for global land areas. Int. J. Climatol. 37 (12), 4302–4315.
Garg, K.K., Singh, R., Anantha, K.H., Singh, A.K., Akuraju, V.R., Barron, J., Dev, I., Tewari, R.K., Wani, S.P., Dhyani, S.K., Dixit, S., 2020. Building climate resilience in degraded agricultural landscapes through water management: a case study of Bundelkhand region, Central India. J. Hydrol. 591, 125592.
Ge, Y., Thomasson, J.A., Morgan, C.L., Searcy, S.W., 2007. VNIR diffuse reflectance spectroscopy for agricultural soil property determination based on regression-kriging. Trans. ASABE 50 (3), 1081–1092.
Ghosh, A., Singh, A.K., Kumar, S., Manna, M.C., Jha, P., Bhattacharyya, R., Sannagoudar, M.S., Singh, R., Chaudhari, S.K., Kumar, R.V., 2021. Do moisture conservation practices influence stability of soil organic carbon and structure? Catena 199, 105127.
Grimm, R., Behrens, T., 2010. Uncertainty analysis of sample locations within digital soil mapping approaches. Geoderma 155 (3–4), 154–163.
Grinand, C., Barthès, B.G., Brunet, D., Kouakoua, E., Arrouays, D., Jolivet, C., Caria, G., Bernoux, M., 2012. Prediction of soil organic and inorganic carbon contents at a national scale (France) using mid-infrared reflectance spectroscopy (MIRS). Eur. J. Soil Sci. 63 (2), 141–151.
Grunwald, S., Congrong, Y.U., Xiong, X., 2018. Transferability and scalability of soil total carbon prediction models in Florida, USA. Pedosphere 28 (6), 856–872.
Guerrero, C., Zornoza, R., Gómez, I., Mataix-Beneyto, J., 2010. Spiking of NIR regional models using samples from target sites: effect of model size on prediction accuracy. Geoderma 158 (1–2), 66–77.
Hansen, H.O., 2024. Megatrends in Agriculture, Food Industry and Food Markets: An Empirical and Holistic Approach (p. 410). Springer Nature.
Hanway, J.J., Heidel, H., 1952. Soil analysis methods as used in Iowa state college soil testing laboratory. Iowa Agric. 57 (1952), 1–31.
Heuvelink, G.B., 2018. Uncertainty and uncertainty propagation in soil mapping and modelling. In: Pedometrics. Springer International Publishing, Cham, pp. 439–461.
Heuvelink, G.B., Burrough, P.A., Stein, A., 1989. Propagation of errors in spatial modelling with GIS. International Journal of Geographical Information System 3 (4), 303–322.
Islam, K., McBratney, A., Singh, B., 2005. Rapid estimation of soil variability from the convex hull biplot area of topsoil ultra-violet, visible and near-infrared diffuse reflectance spectra. Geoderma 128 (3–4), 249–257.
Jolivet, C., Arrouays, D., Boulonne, L., Ratié, C. and Saby, N., 2006. Le réseau de mesures de la qualité des sols de France (RMQS). Etat d'avancement et premiers résultats. Etude et Gestion des Sols, 13(3), pp.149-164.
Keren, R., 1996. Boron. In: Sparks, D. L., Page, A. L. (Eds.), Methods of soil analysis, part 3 chemical methods. Soil Science Society of America and American Society of Agronomy, (pp. 603–626).
Kiran, A.P., Kudesia, R., 2009. Soil quality of degraded land of Bundelkhand region with special reference to Jhansi district of Uttar Pradesh. J. Phytology 1 (5).
Kumar, D., Ranjan, R., Meena, M.K., Yadav, R.S., Gupta, G., Jinger, D., Yadav, D., Pramanik, M., 2021. Exploring conservation agricultural practices in Bundelkhand region, Central India. In: Conservation Agriculture: A Sustainable Approach for Soil Health and Food Security: Conservation Agriculture for Sustainable Agriculture. Singapore, Springer Singapore, pp. 195–222.
Kursa, M.B., Rudnicki, W.R., 2010. Feature selection with the Boruta package. J. Stat. Softw. 36, 1–13.
Lamsal, S., 2009. Visible near-infrared reflectance spectrocopy for geospatial mapping of soil organic matter. Soil Sci. 174 (1), 35–44.
Lawrence, I., Lin, K., 1989. A concordance correlation coefficient to evaluate reproducibility. Biometrics 255–268.
Liaw, A., Wiener, M., 2002. Classification and regression by randomForest. R News 2 (3), 18–22.
Liu, Y., Shi, Z., Zhang, G., Chen, Y., Li, S., Hong, Y., Shi, T., Wang, J., Liu, Y., 2018. Application of spectrally derived soil type as ancillary data to improve the estimation of soil organic carbon by using the chinese soil vis-NIR spectral library. Remote Sens. (Basel) 10 (11), 1747.
Long, M., Yue, T., Xu, Z., Guo, J., Luo, J., Guo, X., Zhao, X., 2023. Improved Soil Organic Carbon Prediction in a Forest Area by Near-Infrared Spectroscopy: Spiking of a Soil Spectral Library. Forests 14 (1), 118.
Luce, M.S., Ziadi, N., Viscarra Rossel, R.A., 2022. GLOBAL-LOCAL: a new approach for local predictions of soil organic carbon content using large soil spectral libraries. Geoderma 425, 116048.
Ma, Y., Minasny, B., Malone, B.P., Mcbratney, A.B., 2019. Pedology and digital soil mapping (DSM). Eur. J. Soil Sci. 70 (2), 216–235.
Ma, Y., Minasny, B., McBratney, A., Poggio, L., Fajardo, M., 2021. Predicting soil properties in 3D: should depth be a covariate? Geoderma 383, 114794.
Majeed, I., Garg, K.K., Venkataradha, A., Purushothaman, N.K., Roy, S., Reddy, N.N., Singh, R., Anantha, K.H., Dixit, S., Das, B.S., 2023. Diffuse reflectance spectroscopy (DRS) for rapid soil testing and soil quality assessment in smallholder farms. Eur. J. Soil Sci. 74 (2), e13358.
McBratney, A.B., Santos, M.M., Minasny, B., 2003. On digital soil mapping. Geoderma 117 (1–2), 3–52.
Meinshausen, N., 2006. Quantile regression forests. Journal of Machine Learning Research, 7 (6) (2006), pp. 983-999.
Minasny, B., Tranter, G., McBratney, A.B., Brough, D.M., Murphy, B.W., 2009. Regional transferability of mid-infrared diffuse reflectance spectroscopic prediction for soil chemical properties. Geoderma 153 (1–2), 155–162.
Mulder, V.L., Lacoste, M., Richer-de-Forges, A.C., Arrouays, D., 2016. GlobalSoilMap France: High-resolution spatial modelling the soils of France up to two meter depth. Sci. Total Environ. 573, 1352–1369.
Nelson, M.A., Bishop, T.F.A., Triantafilis, J., Odeh, I.O.A., 2011. An error budget for different sources of error in digital soil mapping. Eur. J. Soil Sci. 62 (3), 417–430.
Ng, W., Minasny, B., Jones, E., McBratney, A., 2022. To spike or to localize? strategies to improve the prediction of local soil properties using regional spectral library. Geoderma 406, 115501.
Ng, W., Minasny, B., Montazerolghaem, M., Padarian, J., Ferguson, R., Bailey, S., McBratney, A.B., 2019. Convolutional neural network for simultaneous prediction of several soil properties using visible/near-infrared, mid-infrared, and their combined spectra. Geoderma 352, 251–267.
Olsen, S.R., Sommers, L.E., 1982. Phosphorus. In: Page, A.L., Miller, R.H., Keeney, D.R. (Eds.), In Methods of Soil Analysis. Part II, (2nd ed.,. American Society of Agronomy and Soil Science Society of America, pp. 403–430.

Padarian, J., Minasny, B., McBratney, A.B., 2017. Chile and the Chilean soil grid: a contribution to GlobalSoilMap. Geoderma Reg. 9, 17–28.
Padarian, J., Minasny, B., McBratney, A.B., 2019. Using deep learning for digital soil mapping. Soil 5 (1), 79–89.
Padarian, J., Stockmann, U., Minasny, B., McBratney, A.B., 2022. Monitoring changes in global soil organic carbon stocks from space. Remote Sens. Environ. 281, 113260.
Poggio, L., De Sousa, L.M., Batjes, N.H., Heuvelink, G.B., Kempen, B., Ribeiro, E., Rossiter, D., 2021. SoilGrids 2.0: producing soil information for the globe with quantified spatial uncertainty. Soil 7 (1), 217–240.
Posit team (2024). RStudio: Integrated Development Environment for R. Posit Software, PBC, Boston, MA. URL http://www.posit.co/.
Prasad, M., Mahawer, S.K., Govindswamy, P., Kumar, S., 2020. Assessment of soil fertility attributes in selected districts of Bundelkhand region of Central India. Current Journal of Applied Science and Technology 39 (48), 326–334.
Purushothaman, N.K., Garg, K.K., Venkataradha, A., Anantha, K.H., Singh, R., Jat, M.L., Das, B.S., 2024. Applicability of calibrated diffuse reflectance spectroscopy models across spatial and temporal boundaries. Geoderma 449, 117012.
Purushothaman, N.K., Swan, T., Singh, K., Fidelis, C., Majeed, I., Yinil, D., Minasny, B., Das, B.S., Field, D.J., 2025. Diffuse Reflectance Spectroscopy for Soil Testing under Different Soil Nutrient Management in Cocoa Production Systems. Soil Use Manag. 41 (2), e70094.
R Core Team, 2023. R: a language and environment for statistical computing. R Foundation for Statistical Computing, Vienna, Austria https://www.R-project.org/.
Reddy, N.N., Das, B.S., 2023. Digital soil mapping of key secondary soil properties using pedotransfer functions and Indian legacy soil data. Geoderma 429, 116265.
Reddy, N.N., Chakraborty, P., Roy, S., Singh, K., Minasny, B., McBratney, A.B., Biswas, A., Das, B.S., 2021. Legacy data-based national-scale digital mapping of key soil properties in India. Geoderma 381, 114684.
Sarathjith, M.C., Das, B.S., Wani, S.P., Sahrawat, K.L., 2014. Dependency measures for assessing the covariation of spectrally active and inactive soil properties in diffuse reflectance spectroscopy. Soil Sci. Soc. Am. J. 78 (5), 1522–1530.
Sarkar, D., Haldar, A., 2005. Physical and chemical methods in soil analysis: fundamental concepts of analytical chemistry and instrumental techniques. New Age. International.
Savitzky, A., Golay, M.J., 1964. Smoothing and differentiation of data by simplified least squares procedures. Anal. Chem. 36 (8), 1627–1639.
Sendhil, R., Kumar, A., Sharma, A.K., Jasrotia, P., Gupta, O.P., Meena, R.P., Singh, S., Singh, G.P., 2018. Strengthening value chain in wheat and barley for doubling farmers income. Directorate of Extension, Department of Agriculture Cooperation & Farmers Welfare and ICAR-Indian Institute of Wheat and Barley Research, pp.1–144.
Sharma, R.S., Mondal, M.E.A., 2018. Evolution of the Indian Shield: a new approach. In: Geological Evolution of the Precambrian Indian Shield. Springer International Publishing, Cham, pp. 17–38.
Shepherd, K.D., Walsh, M.G., 2002. Development of reflectance spectral libraries for characterization of soil properties. Soil Sci. Soc. Am. J. 66 (3), 988–998.
Shepperd, M., MacDonell, S., 2012. Evaluating prediction systems in software project estimation. Inf. Softw. Technol. 54 (8), 820–827.
Silhavy, P., Silhavy, R., Prokopova, Z., 2021. Spectral clustering effect in software development effort estimation. Symmetry 13 (11), 2119.
Singh, A.K., Raj, B., Tiwari, A.K., Mahato, M.K., 2013. Evaluation of hydrogeochemical processes and groundwater quality in the Jhansi district of Bundelkhand region, India. Environmental Earth Sciences 70 (3), 1225–1247.
Singh, R., Akuraju, V., Anantha, K.H., Garg, K.K., Barron, J., Whitbread, A.M., Dev, I., Dixit, S., 2022. Traditional rainwater management (haveli cultivation) for building system level resilience in a fragile ecosystem of Bundelkhand region, Central India. Front. Sustainable Food Syst. 6, 826722.
Somarathna, P.D.S.N., Minasny, B., Malone, B.P., Stockmann, U., McBratney, A.B., 2018. Accounting for the measurement error of spectroscopically inferred soil carbon data for improved precision of spatial predictions. Sci. Total Environ. 631, 377–389.
Stenberg, B., Rossel, R.A.V., Mouazen, A.M., Wetterlind, J., 2010. Visible and near infrared spectroscopy in soil science. Adv. Agron. 107, 163–215.
Stevens, A., Ramirez-Lopez, L., 2022. An introduction to the prospectr package. R package Vignette R package version 0.2.6. https://cran.r-project.org/web/packages/prospectr/vignettes/prospectr.html.
Stockmann, U., Padarian, J., McBratney, A., Minasny, B., de Brogniez, D., Montanarella, L., Hong, S.Y., Rawlins, B.G., Field, D.J., 2015. Global soil organic carbon assessment. Glob. Food Sec. 6, 9–16.
Tóth, G., Jones, A., Montanarella, L., 2013. The LUCAS topsoil database and derived information on the regional variability of cropland topsoil properties in the European Union. Environ. Monit. Assess. 185 (9), 7409–7425.
Vaysse, K., Lagacherie, P., 2017. Using quantile regression forest to estimate uncertainty of digital soil mapping products. Geoderma 291, 55–64.
Viscarra Rossel, R.A., McBratney, A.B., 2008. Diffuse reflectance spectroscopy as a tool for digital soil mapping. In: Digital Soil Mapping with Limited Data. Springer, Netherlands, Dordrecht, pp. 165–172.
Viscarra Rossel, R.A., Webster, R., 2012. Predicting soil properties from the Australian soil visible–near infrared spectroscopic database. Eur. J. Soil Sci. 63 (6), 848–860.
Viscarra Rossel, R.A., Behrens, T., Ben-Dor, E., Brown, D.J., Demattê, J.A.M., Shepherd, K.D., Shi, Z., Stenberg, B., Stevens, A., Adamchuk, V., Aïchi, H., 2016. A global spectral library to characterize the world's soil. Earth Sci. Rev. 155, 198–230.
Viscarra Rossel, R.A., Shen, Z., Lopez, L.R., Behrens, T., Shi, Z., Wetterlind, J., Sudduth, K.A., Stenberg, B., Guerrero, C., Gholizadeh, A., Ben-Dor, E., 2024. An imperative for soil spectroscopic modelling is to think global but fit local with transfer learning. Earth Sci. Rev. 254, 104797.
Viscarra Rossel, R., Walvoort, D.J.J., McBratney, A.B., Janik, L.J., Skjemstad, J.O., 2006. Visible, near infrared, mid infrared or combined diffuse reflectance spectroscopy for simultaneous assessment of various soil properties. Geoderma 131 (1–2), 59–75.
Viscarra Rossel, R.A., Behrens, T., Ben-Dor, E., Chabrillat, S., Demattê, J.A.M., Ge, Y., Gomez, C., Guerrero, C., Peng, Y., Ramirez-Lopez, L., Shi, Z., 2022. Diffuse reflectance spectroscopy for estimating soil properties: a technology for the 21st century. Eur. J. Soil Sci. 73 (4), e13271.
Viscarra Rossel, R.A., Webster, R., Bui, E.N., Baldock, J.A., 2014. Baseline map of organic carbon in Australian soil to support national carbon accounting and monitoring under climate change. Glob. Chang. Biol. 20 (9), 2953–2970.
Wadoux, A.M.C., Minasny, B., McBratney, A.B., 2020. Machine learning for digital soil mapping: applications, challenges and suggested solutions. Earth Sci. Rev. 210, 103359.
Wadoux, A.M.C., Padarian, J., Minasny, B., 2019. Multi-source data integration for soil mapping using deep learning. Soil 5 (1), 107–119.
Walkley, A. and Black, I.A., 1934. An examination of the Degtjareff method for determining soil organic matter, and a proposed modification of the chromic acid titration method. Soil Science, 37 (1) (1934), pp. 29-38.
Wandrey, C.J. and Law, B.E., 1997. Open-File Report 97-470C. US Geological Survey Open File Report, 97, p.470C.
Wang, B., Gray, J.M., Waters, C.M., Anwar, M.R., Orgill, S.E., Cowie, A.L., Feng, P., Li Liu, D., 2022. Modelling and mapping soil organic carbon stocks under future climate change in south-eastern Australia. Geoderma 405, 115442.
Yamazaki, D., Ikeshima, D., Tawatari, R., Yamaguchi, T., O'Loughlin, F., Neal, J.C., Sampson, C.C., Kanae, S., Bates, P.D., 2017. A high accuracy map of global terrain elevations. Geophys. Res. Lett. 44, 5844–5853.
Zayani, H., Fouad, Y., Michot, D., Kassouk, Z., Lili-Chabaane, Z., Walter, C., 2023. Detecting the temporal trend of cultivated soil organic carbon content using visible near infrared spectroscopy. J. Near Infrared Spectrosc. 31 (5), 241–255.